Title
Pairing Centers mediate meiotic chromosome dynamics in C. elegans

Author
Rillo, Regina

Publication Date
2011

Peer reviewed|Thesis/dissertation

Pairing Centers mediate meiotic chromosome dynamics in *C. elegans*

By

Regina Rillo

A dissertation submitted in partial satisfaction of the

requirements for the degree of

Doctor of Philosophy

in

Molecular and Cell Biology

in the

Graduate Division

of the

University of California, Berkeley

Committee in charge:

Professor Abby F. Dernburg, Chair
Professor Barbara Meyer
Professor Zac Cande
Professor Jan Liphardt

Fall 2011

Abstract

Pairing Centers mediate meiotic chromosome dynamics in *C. elegans*

by

Regina Rillo

Doctor of Philosophy in Molecular and Cell Biology

University of California, Berkeley

Professor Abby F. Dernburg, Chair

All sexually reproducing animals depend on meiosis, the specialized cell division in which haploid gametes are produced from a diploid germ cell. Meiotic cells undergo one round of replication followed by two rounds of division. A distinctive feature of the first meiotic prophase is the establishment of physical linkages, via crossover recombination, between homologous chromosomes, which are essential for their proper segregation at metaphase I. Prior to the recombination step, however, homologous chromosomes must overcome the problem of finding and recognizing their appropriate partner within the nuclear volume, a process called homolog pairing. Transient interactions between paired homologs are further stabilized by a process called synapsis, in which the synaptonemal complex polymerizes along the entire length of paired chromosome axes. My research aims to address central questions to our understanding of the meiotic process: how do homologous chromosomes find and recognize their correct partner and how is synapsis regulated so that it occurs only between properly paired homologs. In Chapter 1, I present data that Pairing Centers are essential to facilitate proper connections between chromosomes and the nuclear envelope by recruiting a polo-like kinase. In Chapter 2, I identify novel meiotic mutants through a candidate screen and present my preliminary characterization of their meiotic defects. I further describe tools to visualize their chromosome dynamics *in vivo.*

I dedicate this thesis to my mom and dad,
Ken and Beth Giorgi,
for their continuous support
throughout my journey in graduate school,
and to my husband,
Eric Bohn,
who often encouraged me to
“make lots of breakthroughs in science”.

Table of Contents

List of Figures

List of Tables

General Introduction

Meiosis: an overview

All sexually reproducing animals rely on the process of meiosis to generate haploid gametes from diploid progenitor cells. Sexual reproduction serves two purposes; the reduction in chromosome number is important as it maintains the correct ploidy of the organism upon fertilization, at the same time shuffling genetic information to create allelic combinations driving natural selection and evolution. Meiotic cells undergo one round of replication followed by two rounds of cell division. Homologous chromosomes are segregated in the first reductional division (meiosis I), followed by sister chromatid segregation at the second equational divsion (meiosis II). The resulting gametes contain half the number of chromosomes of the progenitor cells.

Defects in meiosis give rise to aneuploid gametes, which frequently results in embryonic lethality upon fertilization. Humans tolerate some rare cases of aneuploidy and among those rare cases that reach full term, like Trisomy 21 and Klinefelter's Syndrome, the fetus is born with various developmental defects and abnormalities (Hassold & Hunt, 2001). More often, aneuploidy results in miscarriages. Therefore it is essential that faithful chromosome segregation occur during meiosis to produce gametes containing an accurate number of chromosomes.

Although the equational division of meiosis is similar to the process of a mitotic division, the reductional division is unique in that it requires pairs of homologous chromosomes to become physically linked together to enable their proper alignment, bi-orientation and, ultimately, segregation at metaphase I. A series of important events must occur successfully prior to the first meiotic division. During prophase, chromosomes must find and recognize their unique homologous partner. Transient homologous interactions are reinforced during synapsis, when the synaptonemal complex (SC) is assembled along the entire length of the homolog pair. Homologs exchange genetic material, and physical linkages are created via crossover recombination. How chromosomes recognize their unique partner and how pairing and synapsis are coordinated to ensure that synapsis occurs discriminately between paired homologs remain big mysteries in the meiosis field.

The Meiotic Bouquet and Homolog Pairing

In many organisms, meiotic entry coincides with dramatic chromosome reorganization. Chromosome ends become associated with the nuclear envelope forming a cluster resembling a bouquet of flowers, which led to the term chromosomal 'bouquet'. Initial observations that chromosomes interact with the nuclear envelope during meiotic prophase were first reported more than a hundred years ago by Gustav Eisen who studied salamander meiosis (Eisen, 1900). But it

was more than a decade later when Jozsef Gelei carefully described different chromosome morphologies in flatworm meiosis that the bouquet conformation was associated with the reduction of chromosome number (reviewed in Scherthan, 2001). Although it is now accepted as a widely conserved aspect of meiotic prophase, how the bouquet contributes to homolog pairing and synapsis is still not completely understood. While initially suspected to promote pairing by allowing homology search to occur in a two-dimensional space instead of the three-dimensional nuclear volume, more recent work has revealed that this view may be over-simplified; chromosome tethering may function at both promoting homologous interactions as well as restricting promiscuous ones between nonhomologous chromosomes.

Components of the meiotic bouquet in various organisms

Much of what is known about the molecular components of the meiotic bouquet came from studies in the fission yeast *S. pombe.* Like most organisms, *S. pombe* rely on normal telomere structure to mediate interactions between chromosomes and the nuclear envelope. In this organism, telomere proteins associate with a protein bridge to link chromosomes to the spindle-pole body (SPB) and cytoplasmic microtubules. Mutations in genes encoding telomere-associated proteins Taz1p and Rap1p, among others, disrupt bouquet formation and lead to missegregation of homologous chromosomes (Chikashige & Hiraoka, 2001; Cooper et al., 1998; Nimmo et al., 1998). Bridging telomeres to the SPB is a complex of meiosis-specific proteins including Bqt1, 2, 3, and 4 (Chikashige et al., 2006; Chikashige et al., 2009). A deletion in any of the four Bqt proteins leads to a loss of proper bouquet formation and defects in viable spore formation and meiotic recombination frequency, highlighting the requirement for a normal meiotic bouquet to promote proper meiotic segregation.

Telomere clustering and the dynein-driven “horsetail” movement of the entire nucleus during meiotic prophase play a major role in chromosome alignment and homologous recombination in *S. pombe* (Ding et al., 1998; Ding et al., 2004; Niwa et al., 2000). At the nuclear envelope, a complex of membrane proteins, including Sad1p and Kms1p, bridge connections between telomeres and the microtubule cytoskeleton (Hagan & Yanagida, 1995; Shimanuki et al., 1997). A founding member of the SUN domain family of proteins (named after founding members Sad1 and UNC-84), Sad1p is a transmembrane protein located at the inner nuclear membrane of the nuclear envelope and contains a highly conserved domain at its C-terminus (Starr & Fridolfsson, 2010). This SUN domain is believed to reside in the lumen of the nuclear envelope, the space between the inner and outer nuclear membrane, where it interacts with a member of the KASH domain family, Kms1p. KASH domain (Klarsicht, ANC-1, Syne Homology) proteins are C-tailed-anchored proteins that reside in the outer nuclear membrane and often directly interact with components of the cytoskeleton (reviewed in Starr, 2011).

In the budding yeast *S. cerevisiae*, telomeres also cluster at the nuclear periphery though not as intimately connected to the SPB. Ndj1, a meiosis-specific

telomere-associated protein, directly interacts with the SPB component Mps3, and together with Csm4 forms the meiotic bouquet in this organism (Conradet al., 1997; Conrad et al., 2007; Kosaka et al., 2008; Trelles-Sticken et al., 2000; Wanat et al., 2008). Csm4 is not strictly required for telomere attachment, however, as chromosomes remain associated with the nuclear envelope in its absence but fail to cluster (Kosaka et al., 2008). The meiotic bouquet in budding yeast seem to play a less important role in early prophase, as mutations in Ndj1 only modestly decreased homologous associations and meiotic recombination (Conrad et al., 2007; Goldman & Lichten, 2000). Interestingly, *ndj1* mutants also display increased ectopic recombination which suggests a defect in homolog recognition. Although known molecular players of the meiotic bouquet have been most extensively studied in fungi species, telomeres in a wide variety of other organisms have been implicated in bouquet formation through cytology. Telomere bouquets are also found in mice, wheat, and maize (Bass et al., 2000; Martínez-Pérez et al., 1999; Scherthan et al., 1996).

Unlike yeast and other organisms, the meiotic bouquet in *C. elegans* is mediated by specific *cis*-acting regions on each chromosome known as Pairing Centers (PCs) (MacQueen et al., 2005). Each Pairing Center contains a high density of specific DNA binding motifs that is recognized by a member of a family of zinc-finger proteins (ZnFs) (Phillips et al., 2005; Phillips & Dernburg, 2006; Phillips et al., 2009). PC ZnFs recruit chromosome ends to the nuclear envelope where they associate with SUN-1, an inner nuclear membrane protein with a highly conserved SUN domain, and ZYG-12, a KASH domain-containing protein at the outer nuclear membrane (Malone et al., 2003; Penkner et al., 2007; Sato et al., 2009). Studies revealed that the meiotic bouquet in *C. elegans* is essential for proper homolog pairing and synapsis. Deletions of individual ZnF proteins abrogate pairing and synapsis of the corresponding chromosome(s) (Phillips et al., 2005; Phillips & Dernburg, 2006). And mutations in *sun-1* or *zyg-12* lead to synapsis between nonhomologous chromosomes (Penkner et al., 2007; Sato et al., 2009).

Meiotic chromosome dynamics

An important advantage of establishing the chromosomal bouquet during meiotic prophase is to connect chromosomes to the cytoskeleton, where it can use forces generated by associated motors to drive chromosome movement. The most extreme example of chromosome dynamics are observed in *S. pombe.* In this organism, the entire nucleus oscillates throughout prophase while telomeres are tightly clustered at the SPB (Ding et al., 1998). By directly analyzing associations between specific chromosomal loci in wild-type and various mutant cells, Ding et al. revealed that homologous loci associate and disassociate repeatedly throughout meiosis and that the frequency of associations increase with meiotic progression (Ding et al., 2004). In the absence of *Rec12,* the conserved topoisomerase required for programmed double-strand breaks, homologous loci associate with wild-type kinetics but are short-lived and fail to

increase with meiotic progression, indicating that early transient and dynamic pairing interactions between homologous loci do not require recombination but their eventual stabilization does. Cytoplasmic dynein, on the other hand, is essential for early homolog pairing and alignment. Mutations that disrupt cytoplasmic dynein and abrogate nuclear oscillations lead to a severe decrease in early homologous associations and recombination (Ding et al., 2004; Yamamoto et al., 1999). Loci at chromosomal arms and centromeres all show a decrease in homologous associations in *dhc1*$^{-}$ mutants (Ding et al., 2004). Interestingly, mutations that disrupt telomere attachment, such as in *taz1*$^{-}$*,* lead to less severe defects in homolog pairing compared to mutations that abrogate nuclear oscillations (Ding et al., 2004). Furthermore, an increase in ectopic recombination is observed in the absence of telomere attachment but not in oscillation-defective mutants, which may indicate a specific role for telomere attachment in homolog alignment while the role of nuclear oscillation may be to promote general encounters between chromosomes (Ding et al., 2004). Taken together, the meiotic bouquet in *S. pombe* facilitates motion that promotes homologous interactions while limiting nonhomologous ones.

In the budding yeast *S. cerevisiae*, the actin cytoskeleton plays a major role in bouquet formation and meiotic chromosome dynamics (Trelles-Sticken et al., 2005). Live imaging of chromosomes in this organism revealed telomere-led rapid prophase movements (RPMs), which frequently exceeded 1μm/s, that are dependent on meiotic bouquet genes *NDJ1, MPS3* and *CSM4* (Conrad et al., 2008). In bouquet mutants, RPMs are reduced, reflecting the inability of chromosomes to establish stable associations with the nuclear envelope and the cytoskeletal components that generate the force required for these movements (Conrad et al., 2008). By using Abp140-GFP, a probe which allows live imaging of the actin cytoskeleton, Koszul et al. showed that large actin cables “hug” or form near the periphery of the outer nuclear envelope and that chromosome motion is correlated with their tracks (Koszul et al., 2008). They observed instances in which a group of chromosomes, or at times a single chromosome, moves along an outward-directed path. Interestingly, telomeres exhibit RPMs regardless of their pairing status. In fact, paired telomere ends undergo RPMs at a higher velocity than unpaired telomeres, suggesting a role for RPMs not in facilitating homologous interactions but in disrupting nonhomologous ones, an idea that is supported by the fact that pairing of telomeres was increased in the absence of telomere attachment and recombination in the *ndt80Δ* background (Michael N Conrad et al., 2008).

Another possible role for the meiotic bouquet and chromosome dynamics were derived from studies of meiosis in maize. Live imaging analysis revealed that chromosomes also undergo rapid chromosome motion in early prophase which are dependent on both the actin and microtubule cytoskeleton (Sheehan and Pawlowski, 2009). A mutation in the gene *pam1,* results in defects in telomere clustering even when telomeres are associated with the nuclear envelope (Golubovskaya et al., 2002). Furthermore, nonhomologous synapsis and

chromosomal interlocks were increased in the *pam1* mutant, suggesting that another function of the bouquet may be to resolve interlocks between chromosomes.

Like *S. pombe, C. elegans* meiosis depend on the microtubule cytoskeleton for proper homolog pairing and synapsis. Cytoplasmic dynein, which associates with chromosomes in concentrated patches at the nuclear envelope, is not essential for homolog pairing but is required for its normal kinetics; various dynein mutants exhibit a delay in homolog pairing (Sato et al., 2009). In colchicine-injected animals, however, homolog pairing is completely abrogated, suggesting a role for other microtubule-associated motors, like kinesins, in promoting homologous encounters (Sato et al., 2009). Live imaging of the X chromosome was achieved by the expression of a GFP-tagged HIM-8 in the germline. Using this tool, Wynne et al. showed that chromosomes undergo processive chromosome motions (PCMs), characterized by the persistent movement of chromosomes in one direction for up to several seconds. PCMs are dynein-dependent and occur regardless of pairing status in the transition zone but are absent in pachytene (Wynne et al., unpublished) They postulate that PCMs, while not required for pairing, may function in the subsequent initiation of synapsis.

General model for the meiotic bouquet

Whether by telomeres or other distinct chromosomal regions, connections between chromosomes and the nuclear envelope remain conserved across various organisms, and mutations affecting bouquet formation lead to various defects in meiotic prophase. While meiosis-specific proteins that bridge the interactions between chromosomes and the nuclear envelope lack conservation amongst species, SUN/KASH proteins at the nuclear envelope and their connections with the cytoskeleton (microtubules or actin) are highly conserved. Studies of the meiotic bouquet in various organisms emphasize the significant role that chromosome clustering plays in homolog alignment and thereby in pairing.

Synapsis

In most organisms, transient interactions during early prophase are potentially stabilized by the formation of the SC between associated chromosome axes. This process is called synapsis, and it results in the proper chromosomal context in which crossover recombination can ensue between homologs. *S. pombe* differs in this aspect of meiosis from other model organisms due to the absence of synapsis during meiotic prophase. It relies heavily on meiotic recombination across its small number of chromosomes (n=3) to stabilize transient chromosome associations. Therefore not much can be said about synapsis in this organism.

Structure of the SC in various organisms

The SC is a tripartite structure that is morphologically conserved from yeast to humans (Wettstein et al., 1984). Although the specific components may differ from organism to organism, the general structure of the SC at the interface of aligned homologous chromosomes remains the same: two rails of the lateral elements (LEs) are connected by proteins that form along them perpendicularly called transverse filaments. LEs are derived from axial elements which load on chromosomes and reorganize their structure upon meiotic entry, including cohesin, condensin, and other meiosis-specific components (reviewed in (Page & Hawley, 2004). Transverse filaments, which assemble between LEs, are composed of central element proteins that are visualized as an electron-dense linear structures between paired chromosome axes in electron microscopy studies.

Initial observations of the SC came from studies in *S. cerevisiae.* The meiotic cohesin complex is loaded on chromosomes to assemble a chromosome core upon which other axial element components bind and assemble. Meiosis-specific protein Hop1 and Red1 form part of the axial element and localize to chromosomes in prophase I (Hollingsworth et al., 1990; Smith & Roeder, 1997). In the absence of meiotic cohesin components Rec8p or Smc3p, Hop1p, or Red1p lateral elements and the SC fail to form (Klein et al., 1999; Loidl et al., 1994; Rockmill & Roeder, 1990). Furthermore, more recent studies show that condensin components were also involved in SC formation. Yu and Koshland isolated a meiosis-specific allele of a condensin component that maintained the ability to condense chromosomes but failed to recruit SC proteins Red1 and Hop1 during meiosis (Yu & Koshland, 2003). Studies in budding yeast revealed that a proper chromosome core consisting of several axial element components are essential for SC formation.

The LEs in other organisms consist of several axial element proteins as well. Hop1 is a member of a family of proteins that share the conserved HORMA domain. Members of this family include the HIM-3 protein and its paralogs HTP-1, -2, and -3 in *C. elegans.* These proteins, along with the meiotic cohesin complex, make up the axial element in this organism. Recent work revealed an hierarchy among these proteins; HTP-3 is recruited to chromosomes and is required for the subsequent loading of the cohesin complex (Severson et al., 2009). Although Rec8p is essential for axial element formation in yeast, axial element proteins associate with chromosomes in the absence of Rec8 protein in *C. elegans* and in other organisms (Bannister et al., 2004; Bhatt et al., 1999; Colaiácovo et al., 2003; Golubovskaya et al., 2006; Severson et al., 2009). Other HORMA domain-containing proteins include HORMAD1 and 2 in mammals (Daniel et al., 2011; Fukuda et al., 2010; Wojtasz et al., 2009) and Asy1 in Arabidopsis (Armstrong et al., 2002), and in conjunction with other components, comprise the axial elements in these organisms.

Central element proteins make up the transverse element which assembles between two stretches of LEs. These include Zip1p in *S. cerevisiae* (Sym et al., 1993), C(3)G in *D. melanogaster,* SCP1 in mammals (Meuwissen et al., 1997) and

SYP-1, -2, -3 and -4 in *C. elegans* (Colaiácovo et al., 2003; MacQueen et al., 2002; Smolikov et al., 2007; Smolikov et al., 2009). While these proteins are not highly conserved across these different organisms, regions of similarity within their structure exist. Primarily, they all contain coiled-coil domains that are flanked by globular domains (reviewed in Zickler & N Kleckner, 1999). Immunolocalization and structure-function studies on their organization suggest that central element proteins interact and dimerize through their coiled-coil domains in an anti-parallel fashion, with their C-termini associating with chromosome axes and the N-termini located at the center of the SC (Dong & Roeder, 2000; Liu et al., 1996; Schmekel et al., 1996). More recent studies using yeast two-hybrid and co-immunoprecipitation analysis to study the four central element proteins found in *C. elegans* showed that the SC has a similar organization to those in rats and mice (Schild-Prüfert et al., 2011). Moreover, central element proteins have the ability to self-aggregate which is evident by the formation of SC polycomplexes in early prophase and in the absence of proper chromosome axes (reviewed in Zickler & Kleckner, 1999). SC polycomplexes are highly organized protein structures, as revealed by electron microscopy images, and require expression of a complete set of central element proteins.

Diverse functions of the SC

The foremost function of the SC is to stabilize transient homologous interactions to permit the maturation of recombination intermediates into crossovers. In yeast, as in most organisms, synapsis initiation is associated with DSB sites in which homologous regions are brought into close contact with each other due to early recombination intermediates. These axial associations can be visualized in a *zip1* mutant and are dependent on Spo11 (Sym et al., 1993). The tight association between synapsis initiation and recombination is evidenced by the fact that several proteins which function during synapsis initiation are also required for CO formation (Börner et al., 2004). Defects in SC formation correlates with a decrease in recombination and aberrant meiotic segregation.

In *C. elegans*, synapsis is independent of recombination, and therefore the SC plays a critical role in maintaining pairing associations. Chromosomes initially pair at their PC region in *syp-1* mutants, but these associations quickly fall apart in pachytene and crossovers fail to form between homologs (MacQueen et al., 2002). In mutants which are defective for homology recognition like *sun-1,* nonhomologous chromosomes undergo synapsis, which also results in achiasmate chromosomes. Hence, it is crucial in this organism that a system is in place to ensure only properly paired homologs are further stabilized by synapsis.

In addition to defects in SC formation, the failure to form proper axial elements during meiotic prophase can lead to defects in homolog pairing in many organisms. Mutations in Red1 or Hop1 results in decreased homologous associations during prophase in yeast (Loidl et al., 1994; Nag et al., 1995). Similarly, pairing is abrogated in a *him-3* or *rec-8* mutant in *C. elegans* (Pasierbek et al., 2001; Zetka et al., 1999) or a *syn1* mutant in Arabidopsis (Bai et al., 1999).

Axial elements have also been implicated in the recombination pathway by promoting the interhomolog repair of DSBs and/or inhibiting sister-chromatid repair. Mutations in *him-3*, an axial element component in *C. elegans*, abrogates pairing and synapsis of homologous chromosomes, but RAD-51 foci marking DSBs disappear with wild-type kinetics, suggesting that DSBs are repaired using the sister chromatid as a template (Couteau et al., 2004). Similar observations were made in *htp-1* mutants, indicating a role for the protein in the barrier to sister-chromatid repair (Martinez-Perez & Villeneuve, 2005).

Recombination

Proper segregation of homologous chromosomes at the first meiotic division requires that homologs be physically linked to each other to facilitate alignment and bi-orientation at metaphase. This is achieved through the formation of crossovers via recombination, a process that is highly conserved throughout various organisms.

The double-strand break repair pathway

The meiotic recombination program proceeds via the formation and repair of DNA double-strand breaks (DSBs). Breaks are catalyzed by the protein Spo11 through a topoisomerase-like transesterase mechanism and often require additional proteins for its activity (reviewed in Keeney, 2001). In budding yeast, at least nine other accessory proteins were implicated in the specific targeting and activity of Spo11p (Aroraet al., 2004; Keeney et al., 1997). Recent work by Panizza et al. (2011) revealed that a complex of accessory proteins including Rec114, Mer2, and Mei4, localizes to chromosome axis sites with Hop1 and Red1 and may function to regulate DSB formation by tethering chromatin loop regions to the axis (Panizza et al., 2011). Such accessory proteins were also found in mammals, suggesting that this feature of DSB regulation may be conserved across diverse species (Kumar et al., 2010). No homologs have been found in *C. elegans* to date, however, which indicates that an alternative mechanism for DSB regulation may exist in this organism, or, more simply, that functional homologs exist but are not readily found by sequence homology alone. Regardless, studies indicate that the role of Spo11 in the initiation of recombination is highly conserved in fission yeast, worms, flies, and mammals (reviewed in Krogh & Symington, 2004).

Upon formation, DSBs are resected to form 3' ssDNA tails that serve as substrates for binding of Dmc1 and/or Rad51 to promote strand exchange with the homologous chromosome. Resection of DSBs depend on a complex of proteins including Rad50, Mre11 and Xrs2/Nbs1 (MRX/N complex). In the absence of its activity, DSB repair is defective and unresected DSBs accumulate in yeast (reviewed in Krogh & Symington, 2004). The MRX/N complex is highly conserved in other organisms, owing to the requirement for resection in DSB repair. *C. elegans mre-11* functions not only in DSB repair but also in DSB formation (Chin &

Villeneuve, 2001; Goodyer et al., 2008). Resulting 3' overhangs are bound by a RecA homolog, Dmc1 or Rad51, to form nucleoprotein filaments which are required to invade intact homologous duplexes. DNA synthesis, second end capture, Holliday junction formation and resolution follow to ensure proper repair of the DSB (Krogh & Symington, 2004).

The observation that the number of DSBs are greater than the number of COs indicate that a significant percentage of DSBs are processed as non-crossovers (NCOs). Recent studies characterized the role of RTEL as an anti-recombinase in humans as well as in *C. elegans*, disassembling strand invasion intermediates and promoting the formation of NCOs (Barber et al., 2008; Youds et al., 2010).

The recombination landscape

Sites of crossovers are not found randomly throughout the genome but instead at preferential chromosomal regions termed "hotspots" (Kauppi et al., 2004). This is largely due to the nonrandom distribution of DSBs which in turn dictates distribution of COs (Baudat & Nicolas, 1997; reviewed in Petes, 2001). DNA sequence and chromosome structure both contribute to DSB distribution across the genome.

In yeast and mice, trimethylation of lysine 4 of histone H3 (H3K4me3) is a common feature of recombination hotspots (Borde et al., 2009; Buard et al., 2009). The eventual identification of the *Prdm9* gene further elucidated how hotspots are specified based on DNA sequence as well as chromosome structure (Baudat et al., 2010; Parvanov et al., 2010). The gene encodes for a zinc finger protein containing a histone methyltransferase which is specifically involved in trimethylation and is expressed in early meiosis. Studies in the distribution of human hotspots by analysis of linkage disequilibrium revealed a degenerate 13-mer motif that was associated with approximately 40% of hotspots (Myers et al., 2008) and allelic variations found within the zinc fingers of Prdm9 are correlated to the variability of hotspot usage in mice and humans (Baudat et al., 2010; Parvanov et al., 2010). Unpublished results from studies of DSB distribution in *C. elegans* revealed that a specific degenerate motif is also associated with a significant fraction of hotspots (Kotwaliwale et al., unpublished). How the motif may influence hotspot specification in *C. elegans* remains to be determined.

Additional studies in *C. elegans* revealed that a specific condensin complex influences the recombination landscape by controlling axis length and altering the distribution of DSBs (Mets & Meyer, 2009).

Concluding Remarks

Faithful segregation of chromosomes during the first meiotic division requires that mechanisms involving homolog pairing, synapsis and recombination are intact. Previous work in the lab elucidated the role of the meiotic bouquet in homolog pairing and synapsis in *C. elegans*. Still, the mechanism by which

chromosomes form proper attachments to the nuclear envelope was not clear. In Chapter 1, I will describe the design and characterization of a PC-null mutant. This work sheds light on how Pairing Centers function to promote proper meiotic chromosome dynamics that are required for homolog pairing and synapsis. In Chapter 2, I will present the results of a candidate screen for novel meiotic regulators of chromosome dynamics in which I found a handful of mutants that displayed interesting meiotic defects. Furthermore, I will discuss the implementation of LacI/LacO to visualize live chromosome dynamics in *C. elegans.*

References

Armstrong, S. J., Caryl, A. P., Jones, G. H., & Franklin, F. C. H. (2002). Asy1, a protein required for meiotic chromosome synapsis, localizes to axis-associated chromatin in Arabidopsis and Brassica *Journal of cell science*, *115*(Pt 18), 3645–3655.

Arora, C., Kee, K., Maleki, S., & Keeney, Scott. (2004). Antiviral protein Ski8 is a direct partner of Spo11 in meiotic DNA break formation, independent of its cytoplasmic role in RNA metabolism *Molecular cell*, *13*(4), 549–559.

Bai, X., Peirson, B. N., Dong, F., Xue, C., & Makaroff, C. A. (1999). Isolation and characterization of SYN1, a RAD21-like gene essential for meiosis in Arabidopsis *The Plant cell*, *11*(3), 417–430.

Bannister, L. A., Reinholdt, L. G., Munroe, R. J., & Schimenti, J. C. (2004). Positional cloning and characterization of mouse mei8, a disrupted allelle of the meiotic cohesin Rec8 *Genesis (New York, N.Y. : 2000)*, *40*(3), 184–194. doi: 10.1002/gene.20085

Barber, L. J., Youds, J. L., Ward, J. D., McIlwraith, M. J., ONeil, N. J., Petalcorin, M. I. R., Martin, J. S., et al. (2008). RTEL1 maintains genomic stability by suppressing homologous recombination *Cell*, *135*(2), 261–271. doi:10.1016/j.cell.2008.08.016

Bass, H. W., Riera-Lizarazu, O., Ananiev, E. V., Bordoli, S. J., Rines, H. W., Phillips, R. L., Sedat, J. W., et al. (2000). Evidence for the coincident initiation of homolog pairing and synapsis during the telomere-clustering (bouquet) stage of meiotic prophase *Journal of cell science*, *113 (Pt 6)*, 1033–1042.

Baudat, F., Buard, J., Grey, C., Fledel-Alon, A., Ober, C., Przeworski, M., Coop, G., et al. (2010). PRDM9 is a major determinant of meiotic recombination hotspots in humans and mice *Science (New York, N.Y.)*, *327*(5967), 836–840. doi:10.1126/science.1183439

Baudat, F., & Nicolas, A. (1997). Clustering of meiotic double-strand breaks on yeast chromosome III *Proceedings of the National Academy of Sciences of the United States of America*, *94*(10), 5213–5218.

Bhatt, A. M., Lister, C., Page, T., Fransz, P., Findlay, K., Jones, G. H., Dickinson, H. G., et al. (1999). The DIF1 gene of Arabidopsis is required for meiotic chromosome segregation and belongs to the REC8/RAD21 cohesin gene family *The Plant journal : for cell and molecular biology*, *19*(4), 463–472.

Borde, V., Robine, N., Lin, W., Bonfils, S., Géli, V., & Nicolas, A. (2009). Histone H3 lysine 4 trimethylation marks meiotic recombination initiation sites *The EMBO journal*, *28*(2), 99–111. doi:10.1038/emboj.2008.257

Börner, G. V., Kleckner, Nancy, & Hunter, N. (2004). Crossover/noncrossover differentiation, synaptonemal complex formation, and regulatory surveillance at the leptotene/zygotene transition of meiosis *Cell*, *117*(1), 29–45.

Buard, J., Barthès, P., Grey, C., & de Massy, B. (2009). Distinct histone modifications define initiation and repair of meiotic recombination in the mouse *The EMBO journal*, *28*(17), 2616–2624. doi:10.1038/emboj.2009.207
Chikashige, Y, & Hiraoka, Y. (2001). Telomere binding of the Rap1 protein is required for meiosis in fission yeast *Current biology : CB*, *11*(20), 1618–1623.
Chikashige, Yuji, Tsutsumi, C., Yamane, M., Okamasa, K., Haraguchi, T., & Hiraoka, Y. (2006). Meiotic proteins bqt1 and bqt2 tether telomeres to form the bouquet arrangement of chromosomes *Cell*, *125*(1), 59–69. doi:10.1016/j.cell.2006.01.048
Chikashige, Yuji, Yamane, M., Okamasa, K., Tsutsumi, C., Kojidani, T., Sato, M., Haraguchi, T., et al. (2009). Membrane proteins Bqt3 and -4 anchor telomeres to the nuclear envelope to ensure chromosomal bouquet formation *The Journal of cell biology*, *187*(3), 413–427. doi:10.1083/jcb.200902122
Chin, G. M., & Villeneuve, A M. (2001). C. elegans mre-11 is required for meiotic recombination and DNA repair but is dispensable for the meiotic G(2) DNA damage checkpoint *Genes & development*, *15*(5), 522–534. doi:10.1101/gad.864101
Colaiácovo, M. P., MacQueen, A. J., Martinez-Perez, E., McDonald, K., Adamo, A., La Volpe, A., & Villeneuve, A. M. (2003). Synaptonemal complex assembly in C. elegans is dispensable for loading strand-exchange proteins but critical for proper completion of recombination *Developmental cell*, *5*(3), 463–474.
Conrad, M N, Dominguez, A. M., & Dresser, M E. (1997). Ndj1p, a meiotic telomere protein required for normal chromosome synapsis and segregation in yeast *Science (New York, N.Y.)*, *276*(5316), 1252–1255.
Conrad, Michael N, Lee, C.-Y., Chao, G., Shinohara, M., Kosaka, H., Shinohara, A., Conchello, J.-A., et al. (2008). Rapid telomere movement in meiotic prophase is promoted by NDJ1, MPS3, and CSM4 and is modulated by recombination *Cell*, *133*(7), 1175–1187. doi:10.1016/j.cell.2008.04.047
Conrad, Michael N, Lee, C.-Y., Wilkerson, J. L., & Dresser, Michael E. (2007). MPS3 mediates meiotic bouquet formation in Saccharomyces cerevisiae *Proceedings of the National Academy of Sciences of the United States of America*, *104*(21), 8863–8868. doi:10.1073/pnas.0606165104
Cooper, J. P., Watanabe, Y., & Nurse, P. (1998). Fission yeast Taz1 protein is required for meiotic telomere clustering and recombination *Nature*, *392*(6678), 828–831. doi:10.1038/33947
Couteau, F., Nabeshima, K., Villeneuve, Anne, & Zetka, M. (2004). A component of C. elegans meiotic chromosome axes at the interface of homolog alignment, synapsis, nuclear reorganization, and recombination *Current biology : CB*, *14*(7), 585–592. doi:10.1016/j.cub.2004.03.033
Daniel, K., Lange, J., Hached, K., Fu, J., Anastassiadis, K., Roig, I., Cooke, H. J., et al. (2011). Meiotic homologue alignment and its quality surveillance are controlled by mouse HORMAD1 *Nature cell biology*, *13*(5), 599–610. doi:10.1038/ncb2213

Ding, D Q, Chikashige, Y, Haraguchi, T, & Hiraoka, Y. (1998). Oscillatory nuclear movement in fission yeast meiotic prophase is driven by astral microtubules, as revealed by continuous observation of chromosomes and microtubules in living cells *Journal of cell science*, *111 (Pt 6)*, 701–712.
Ding, Da-Qiao, Yamamoto, Ayumu, Haraguchi, Tokuko, & Hiraoka, Yasushi. (2004). Dynamics of homologous chromosome pairing during meiotic prophase in fission yeast *Developmental cell*, *6*(3), 329–341.
Dong, H., & Roeder, G. S. (2000). Organization of the yeast Zip1 protein within the central region of the synaptonemal complex *The Journal of cell biology*, *148*(3), 417–426.
Eisen, A. G. (1900). *The spermatogenesis of Batrachoseps*. Polymorphous Spermatogonia, Auxocytes and Spermatocytes.
Fukuda, T., Daniel, K., Wojtasz, L., Toth, A., & Höög, C. (2010). A novel mammalian HORMA domain-containing protein, HORMAD1, preferentially associates with unsynapsed meiotic chromosomes *Experimental cell research*, *316*(2), 158–171. doi:10.1016/j.yexcr.2009.08.007
Goldman, A. S., & Lichten, M. (2000). Restriction of ectopic recombination by interhomolog interactions during Saccharomyces cerevisiae meiosis *Proceedings of the National Academy of Sciences of the United States of America*, *97*(17), 9537–9542.
Golubovskaya, I. N., Hamant, O., Timofejeva, L., Wang, C.-J. R., Braun, D., Meeley, R., & Cande, W. Z. (2006). Alleles of afd1 dissect REC8 functions during meiotic prophase I *Journal of cell science*, *119*(Pt 16), 3306–3315. doi:10.1242/jcs.03054
Goodyer, W., Kaitna, S., Couteau, F., Ward, J. D., Boulton, S. J., & Zetka, M. (2008). HTP-3 links DSB formation with homolog pairing and crossing over during C. elegans meiosis *Developmental cell*, *14*(2), 263–274. doi:10.1016/j.devcel.2007.11.016
Hagan, I., & Yanagida, M. (1995). The product of the spindle formation gene sad1+ associates with the fission yeast spindle pole body and is essential for viability *The Journal of cell biology*, *129*(4), 1033–1047.
Hassold, T., & Hunt, P. (2001). To err (meiotically) is human: the genesis of human aneuploidy *Nature reviews. Genetics*, *2*(4), 280–291. doi:10.1038/35066065
Hollingsworth, N. M., Goetsch, L., & Byers, B. (1990). The HOP1 gene encodes a meiosis-specific component of yeast chromosomes *Cell*, *61*(1), 73–84.
Kauppi, L., Jeffreys, A. J., & Keeney, Scott. (2004). Where the crossovers are: recombination distributions in mammals *Nature reviews. Genetics*, *5*(6), 413–424. doi:10.1038/nrg1346
Keeney, S. (2001). Mechanism and control of meiotic recombination initiation *Current topics in developmental biology*, *52*, 1–53.
Keeney, S, Giroux, C. N., & Kleckner, N. (1997). Meiosis-specific DNA double-strand breaks are catalyzed by Spo11, a member of a widely conserved protein family *Cell*, *88*(3), 375–384.

Klein, F., Mahr, P., Galova, M., Buonomo, S. B., Michaelis, C., Nairz, K., & Nasmyth, K. (1999). A central role for cohesins in sister chromatid cohesion, formation of axial elements, and recombination during yeast meiosis *Cell*, *98*(1), 91–103. doi:10.1016/S0092-8674(00)80609-1

Kosaka, H., Shinohara, M., & Shinohara, A. (2008). Csm4-dependent telomere movement on nuclear envelope promotes meiotic recombination *PLoS genetics*, *4* (9), e1000196. doi:10.1371/journal.pgen.1000196

Koszul, R., Kim, K. P., Prentiss, M., Kleckner, N, & Kameoka, S. (2008). Meiotic chromosomes move by linkage to dynamic actin cables with transduction of force through the nuclear envelope *Cell*, *133*(7), 1188–1201. doi:10.1016/j.cell.2008.04.050

Krogh, B. O., & Symington, L. S. (2004). Recombination proteins in yeast *Annual review of genetics*, *38*, 233–271. doi:10.1146/annurev.genet.38.072902.091500

Kumar, R., Bourbon, H.-M., & de Massy, B. (2010). Functional conservation of Mei4 for meiotic DNA double-strand break formation from yeasts to mice *Genes & development*, *24*(12), 1266–1280. doi:10.1101/gad.571710

Liu, J. G., Yuan, L., Brundell, E., Björkroth, B., Daneholt, B., & Höög, C. (1996). Localization of the N-terminus of SCP1 to the central element of the synaptonemal complex and evidence for direct interactions between the N-termini of SCP1 molecules organized head-to-head *Experimental cell research*, *226*(1), 11–19. doi:10.1006/excr.1996.0197

Loidl, J, Scherthan, H, & Kaback, D. B. (1994). Physical association between nonhomologous chromosomes precedes distributive disjunction in yeast *Proceedings of the National Academy of Sciences of the United States of America*, *91*(1), 331–334.

MacQueen, A. J., Phillips, C. M., Bhalla, N., Weiser, P., Villeneuve, A. M., & Dernburg, A. F. (2005). Chromosome sites play dual roles to establish homologous synapsis during meiosis in C. elegans *Cell*, *123*(6), 1037–1050. doi:10.1016/j.cell.2005.09.034

MacQueen, A. J., Colaiácovo, M. P., McDonald, K., & Villeneuve, Anne M. (2002). Synapsis-dependent and -independent mechanisms stabilize homolog pairing during meiotic prophase in C. elegans *Genes & development*, *16*(18), 2428–2442. doi:10.1101/gad.1011602

Malone, C. J., Misner, L., Le Bot, N., Tsai, M.-C., Campbell, J. M., Ahringer, J., & White, J. G. (2003). The C. elegans hook protein, ZYG-12, mediates the essential attachment between the centrosome and nucleus *Cell*, *115*(7), 825–836.

Martinez-Perez, E., & Villeneuve, Anne M. (2005). HTP-1-dependent constraints coordinate homolog pairing and synapsis and promote chiasma formation during C. elegans meiosis *Genes & development*, *19*(22), 2727–2743. doi:10.1101/gad.1338505

Martínez-Pérez, E., Shaw, P., Reader, S., Aragón-Alcaide, L., Miller, T., & Moore, G. (1999). Homologous chromosome pairing in wheat *Journal of cell science*, *112 (Pt 11)*, 1761–1769.

Mets, D. G., & Meyer, B. J. (2009). Condensins regulate meiotic DNA break distribution, thus crossover frequency, by controlling chromosome structure *Cell*, *139*(1), 73–86. doi:10.1016/j.cell.2009.07.035
Meuwissen, R. L., Meerts, I., Hoovers, J. M., Leschot, N. J., & Heyting, C. (1997). Human synaptonemal complex protein 1 (SCP1): isolation and characterization of the cDNA and chromosomal localization of the gene *Genomics*, *39*(3), 377–384. doi:10.1006/geno.1996.4373
Myers, S., Freeman, C., Auton, A., Donnelly, P., & McVean, G. (2008). A common sequence motif associated with recombination hot spots and genome instability in humans *Nature genetics*, *40*(9), 1124–1129. doi:10.1038/ng.213
Nag, D. K., Scherthan, H, Rockmill, B., Bhargava, J., & Roeder, G. S. (1995). Heteroduplex DNA formation and homolog pairing in yeast meiotic mutants *Genetics*, *141*(1), 75–86.
Nimmo, E. R., Pidoux, A. L., Perry, P. E., & Allshire, R. C. (1998). Defective meiosis in telomere-silencing mutants of Schizosaccharomyces pombe *Nature*, *392*(6678), 825–828. doi:10.1038/33941
Niwa, O., Shimanuki, M., & Miki, F. (2000). Telomere-led bouquet formation facilitates homologous chromosome pairing and restricts ectopic interaction in fission yeast meiosis *The EMBO journal*, *19*(14), 3831–3840. doi:10.1093/emboj/19.14.3831
Page, S. L., & Hawley, R. S. (2004). The genetics and molecular biology of the synaptonemal complex *Annual review of cell and developmental biology*, *20*, 525–558. doi:10.1146/annurev.cellbio.19.111301.155141
Panizza, S., Mendoza, M. A., Berlinger, M., Huang, L., Nicolas, A., Shirahige, K., & Klein, F. (2011). Spo11-accessory proteins link double-strand break sites to the chromosome axis in early meiotic recombination *Cell*, *146*(3), 372–383. doi:10.1016/j.cell.2011.07.003
Parvanov, E. D., Petkov, P. M., & Paigen, K. (2010). Prdm9 controls activation of mammalian recombination hotspots *Science (New York, N.Y.)*, *327*(5967), 835. doi:10.1126/science.1181495
Pasierbek, P., Jantsch, M., Melcher, M., Schleiffer, A., Schweizer, D., & Loidl, J. (2001). A Caenorhabditis elegans cohesion protein with functions in meiotic chromosome pairing and disjunction *Genes & development*, *15*(11), 1349–1360. doi:10.1101/gad.192701
Penkner, A., Tang, L., Novatchkova, M., Ladurner, M., Fridkin, A., Gruenbaum, Y., Schweizer, D., et al. (2007). The nuclear envelope protein Matefin/SUN-1 is required for homologous pairing in C. elegans meiosis *Developmental cell*, *12*(6), 873–885. doi:10.1016/j.devcel.2007.05.004
Petes, T. D. (2001). Meiotic recombination hot spots and cold spots *Nature reviews. Genetics*, *2*(5), 360–369. doi:10.1038/35072078
Phillips, C. M., Wong, C., Bhalla, N., Carlton, P. M., Weiser, P., Meneely, P. M., & Dernburg, A. F. (2005). HIM-8 binds to the X chromosome pairing center and mediates chromosome-specific meiotic synapsis *Cell*, *123*(6), 1051–1063. doi:10.1016/j.cell.2005.09.035

Phillips, C. M., Meng, X., Zhang, L., Chretien, J. H., Urnov, F. D., & Dernburg, A. F. (2009). Identification of chromosome sequence motifs that mediate meiotic pairing and synapsis in C. elegans *Nature cell biology*, *11*(8), 934–942. doi:10.1038/ncb1904
Phillips, C. M., & Dernburg, A. F. (2006). A family of zinc-finger proteins is required for chromosome-specific pairing and synapsis during meiosis in C. elegans *Developmental cell*, *11*(6), 817–829. doi:10.1016/j.devcel.2006.09.020
Rockmill, B., & Roeder, G. S. (1990). Meiosis in asynaptic yeast *Genetics*, *126*(3), 563–574.
Sato, A., Isaac, B., Phillips, C. M., Rillo, R., Carlton, P. M., Wynne, D. J., Kasad, R. A., et al. (2009). Cytoskeletal forces span the nuclear envelope to coordinate meiotic chromosome pairing and synapsis *Cell*, *139*(5), 907–919. doi:10.1016/j.cell.2009.10.039
Scherthan, H. (2001). *A bouquet makes ends meet Nature reviews. Molecular cell biology* (Vol. 2, pp. 621–627). doi:10.1038/35085086
Scherthan, H, Weich, S., Schwegler, H., Heyting, C., Härle, M., & Cremer, T. (1996). Centromere and telomere movements during early meiotic prophase of mouse and man are associated with the onset of chromosome pairing *The Journal of cell biology*, *134*(5), 1109–1125.
Schild-Prüfert, K., Saito, T. T., Smolikov, S., Gu, Y., Hincapie, M., Hill, D. E., Vidal, M., et al. (2011). Organization of the synaptonemal complex during meiosis in Caenorhabditis elegans *Genetics*, *189*(2), 411–421. doi:10.1534/genetics.111.132431
Schmekel, K., Meuwissen, R. L., Dietrich, A. J., Vink, A. C., van Marle, J., van Veen, H., & Heyting, C. (1996). Organization of SCP1 protein molecules within synaptonemal complexes of the rat *Experimental cell research*, *226*(1), 20–30. doi:10.1006/excr.1996.0198
Severson, A. F., Ling, L., van Zuylen, V., & Meyer, B. J. (2009). The axial element protein HTP-3 promotes cohesin loading and meiotic axis assembly in C. elegans to implement the meiotic program of chromosome segregation *Genes & development*, *23*(15), 1763–1778. doi:10.1101/gad.1808809
Shimanuki, M., Miki, F., Ding, D. Q., Chikashige, Y., Hiraoka, Y., Horio, T., & Niwa, O. (1997). A novel fission yeast gene, kms1+, is required for the formation of meiotic prophase-specific nuclear architecture *Molecular & general genetics : MGG*, *254*(3), 238–249.
Smith, A. V., & Roeder, G. S. (1997). The yeast Red1 protein localizes to the cores of meiotic chromosomes *The Journal of cell biology*, *136*(5), 957–967.
Smolikov, S., Eizinger, A., Hurlburt, A., Rogers, E., Villeneuve, A. M., & Colaiácovo, M. P. (2007). Synapsis-defective mutants reveal a correlation between chromosome conformation and the mode of double-strand break repair during Caenorhabditis elegans meiosis *Genetics*, *176*(4), 2027–2033. doi:10.1534/genetics.107.076968
Smolikov, S., Schild-Prüfert, K., & Colaiácovo, M. P. (2009). A yeast two-hybrid screen for SYP-3 interactors identifies SYP-4, a component required for

synaptonemal complex assembly and chiasma formation in Caenorhabditis elegans meiosis *PLoS genetics*, *5*(10), e1000669. doi:10.1371/journal.pgen.1000669
Starr, D. A. (2011). KASH and SUN proteins *Current biology : CB*, *21*(11), R414–5. doi:10.1016/j.cub.2011.04.022
Starr, D. A., & Fridolfsson, H. N. (2010). Interactions between nuclei and the cytoskeleton are mediated by SUN-KASH nuclear-envelope bridges *Annual review of cell and developmental biology*, *26*, 421–444. doi:10.1146/annurev-cellbio-100109-104037
Sym, M., Engebrecht, J. A., & Roeder, G. S. (1993). ZIP1 is a synaptonemal complex protein required for meiotic chromosome synapsis *Cell*, *72*(3), 365–378.
Trelles-Sticken, E, Dresser, M E, & Scherthan, H. (2000). Meiotic telomere protein Ndj1p is required for meiosis-specific telomere distribution, bouquet formation and efficient homologue pairing *The Journal of cell biology*, *151*(1), 95–106.
Trelles-Sticken, Edgar, Adelfalk, C., Loidl, Josef, & Scherthan, Harry. (2005). Meiotic telomere clustering requires actin for its formation and cohesin for its resolution *The Journal of cell biology*, *170*(2), 213–223. doi:10.1083/jcb.200501042
Wanat, J. J., Kim, K. P., Koszul, R., Zanders, S., Weiner, B., Kleckner, N., & Alani, E. (2008). Csm4, in collaboration with Ndj1, mediates telomere-led chromosome dynamics and recombination during yeast meiosis *PLoS genetics*, *4*(9), e1000188. doi:10.1371/journal.pgen.1000188
Wettstein, von, D., Rasmussen, S. W., & Holm, P. B. (1984). The synaptonemal complex in genetic segregation *Annual review of genetics*, *18*, 331–413. doi:10.1146/annurev.ge.18.120184.001555
Wojtasz, L., Daniel, K., Roig, I., Bolcun-Filas, E., Xu, H., Boonsanay, V., Eckmann, C. R., et al. (2009). Mouse HORMAD1 and HORMAD2, two conserved meiotic chromosomal proteins, are depleted from synapsed chromosome axes with the help of TRIP13 AAA-ATPase *PLoS genetics*, *5*(10), e1000702. doi:10.1371/journal.pgen.1000702
Yamamoto, A, West, R. R., McIntosh, J. R., & Hiraoka, Y. (1999). A cytoplasmic dynein heavy chain is required for oscillatory nuclear movement of meiotic prophase and efficient meiotic recombination in fission yeast *The Journal of cell biology*, *145*(6), 1233–1249.
Youds, J. L., Mets, D. G., McIlwraith, M. J., Martin, J. S., Ward, J. D., ONeil, N. J., Rose, A. M., et al. (2010). RTEL-1 enforces meiotic crossover interference and homeostasis *Science (New York, N.Y.)*, *327*(5970), 1254–1258. doi:10.1126/science.1183112
Yu, H.-G., & Koshland, D. E. (2003). Meiotic condensin is required for proper chromosome compaction, SC assembly, and resolution of recombination-dependent chromosome linkages *The Journal of cell biology*, *163*(5), 937–947. doi:10.1083/jcb.200308027
Zetka, M. C., Kawasaki, I., Strome, S., & Müller, F. (1999). Synapsis and chiasma formation in Caenorhabditis elegans require HIM-3, a meiotic chromosome core

component that functions in chromosome segregation *Genes & development*, *13* (17), 2258–2270.
Zickler, D., & Kleckner, N. (1999). Meiotic chromosomes: integrating structure and function *Annual review of genetics*, *33*, 603–754. doi:10.1146/annurev.genet.33.1.603

Chapter 1: Pairing Centers recruit a Polo-like kinase to mediate meiotic chromosome dynamics

Summary

Previous studies have shown that Pairing Centers and a family of zinc-finger proteins (PC ZnFs) are essential for pairing and synapsis of homologous chromosomes during meiotic prophase. However, the molecular mechanism by which Pairing Centers function to facilitate these critical processes remained a major question in the field of *C. elegans* meiosis. To address this issue, I engineered a deletion allele to characterize meiosis in the absence of all Pairing Center activity by deleting four adjacent genes encoding the PC ZnFs. My work elucidated the role of Pairing Centers in recruiting a polo-like kinase to the nuclear periphery to establish connections between chromosomes and the nuclear envelope.

Introduction

The nematode *C. elegans* is a great model organism to study critical events during meiotic prophase. Meiotic germ cells are arranged in a temporal and spatial manner along a tubular gonad syncytium, such that the progression of the entire meiotic prophase (i.e., pairing, synapsis and recombination) can be visualized in a single gonad. We take advantage of this feature in *C. elegans* and utilize various cytological techniques, in addition to molecular and genetic tools, to address major questions in the field of meiosis.

One such question which remains to be answered is how homologs recognize their partner during the pairing process. Each of the six chromosomes contains a *cis*-acting region on one end called the Pairing Center (PC) (MacQueen et al., 2005; A M Villeneuve, 1994). Previously called Homolog Recognition Regions, PCs were first defined as the region on each chromosome required for pairing and recombination (McKim et al., 1993). Later studies further narrowed down regions sufficient for the pairing activity of each chromosome and revealed that PCs contain a high density of specific DNA binding motifs (Phillips et al., 2009b). PCs are recognized by a family of zinc finger (ZnF) proteins including HIM-8, which specifically binds the X Chromosome, and ZIM-1, -2, and -3 which bind the five autosomes (Phillips et al., 2005; Phillips and Dernburg, 2006). ZIM-2 specifically binds Chromosome V, while ZIM-1 binds Chromosome 2 and 3, and ZIM-3 binds Chromosome 1 and 4. Because different chromosomes are bound by the same ZnF protein, it is clear that the identity of the bound ZnF protein is not sufficient to confer specificity among homologs. Homology recognition must be derived by other factors, presumably at the level of the DNA sequence surrounding the PCs themselves.

The role of PCs was further elucidated by recent work revealing their intimate associations with specific nuclear envelope components during the critical time of pairing and synapsis. Large aggregates or “patches”, which include the inner nuclear member protein SUN-1 and outer nuclear membrane protein ZYG-12, form at the nuclear envelope and colocalize with PC ZnFs upon meiotic entry (Penkner et al., 2007; Sato et al., 2009). Aggregation of SUN-1/ZYG-12 was shown to be dependent on a series of phosphorylated serine residues at the N-terminus of SUN-1 (Penkner et al., 2009). The cytoplasmic domain of ZYG-12 interacts by Y2H with components of cytoplasmic dynein, and consistent with this result, dynein colocalizes with SUN-1/ZYG-12 aggregates in early prophase nuclei (Malone et al., 2003; Sato et al., 2009). Analysis of various mutant alleles lead to the current model of homolog pairing and synapsis in which dynein-based motion at the NE patches is used to assess homology between chromosomes and license subsequent polymerization of the SC between paired homologs (Sato et al., 2009). It was clear that association of PCs with nuclear envelope patches was important for pairing and synapsis. How these connections were properly established, however, was not well-understood.

I addressed this issue by engineering a deletion mutant which abrogates expression of the entire family of PC ZnFs and analyzing its effect on meiotic progression. In the absence of PC ZnFs, meiotic progression was not grossly altered. However, pairing was completely abrogated, as was the formation of NE patches, and aberrant loading of the SC was prominent throughout meiotic prophase. A conserved sequence at the N-termini of PC ZnFs is required to recruit a polo-like kinase to the nuclear envelope, where it facilitates the specific phosphorylation of SUN-1, NE patch formation, and ultimately the establishment of proper chromosome-NE connections.

Results and Discussion

Designing a PC-null mutant strain

I decided to look at meiosis in the absence of all Pairing Center activity by abrogating expression of the ZnF proteins ZIM-1, -2, -3 and HIM-8. The four genes encoding the PC ZnF proteins are closely arranged within a 17-kb region on Chromosome IV. As a consequence, classical genetic techniques could not be used to create a quadruple mutant with existing single deletion alleles. To accomplish such a feat would require a complicated scheme of genetic crosses and an exorbitant amount of time and effort.

Originally the cluster of genes including *zim-1*, *-2*, *-3* and *him-8* was thought to act like an operon, but efforts to create a PC-null mutant by deleting the regulatory region upstream of *zim-1*, the gene located most 5' within the cluster, failed to abrogate expression of the whole gene family. The small deletion specifically abrogated ZIM-1 expression alone, while ZIM-2, -3 and HIM-8 expression was unaffected (Carolyn Marie PhillipsUniversity of California, Berkeley, 2007). This revealed that internal promoters are sufficient to drive expression of the remaining three genes, and other techniques must be utilized to obtain the desired PC-null mutant strain.

Due to the challenges in creating the quadruple by using more conventional methods, I implemented a novel technique called *MosDel* to create a large deletion spanning the open reading frames within the entire gene cluster (Figure 1.1A). This method relied on the presence a Mos1 transposon insertion immediately downstream of *him-8,* the gene most 3' within the cluster. In my hands, *MosDel* worked well and efficiently, and I identified two deletion alleles named *ieDf1* and *ieDf2*.

The deletion alleles were verified in two ways: by PCR and immunofluorescence. A forward primer that recognizes a specific sequence upstream of *zim-1* and a reverse primer that anneals to a sequence in the *unc-119+* gene, yielded a 3.5 kb band in both deletion strains, while no band was amplified in the wild-type and *unc-119(ed3)* control strain (data not shown). To test for expression, I performed immunofluorescence experiments using specific antibodies against HIM-8 and ZIM-2 and confirmed that they were both absent in *ieDf1* and *ieDf2* (Figure 1.1B, data not shown). Preliminary experiments suggested that both deletion alleles behaved in the same manner. Subsequent experiments were done with the *ieDf2* allele that had been outcrossed 3x into the *unc-119(ed3)* strain to get rid of any potential chromosome anomalies resulting from the *MosDel* experiment.

Pairing Centers are required for chromosome reorganization during early meiosis

The formation of the meiotic bouquet is a hallmark of early meiosis in most organisms. In *C. elegans*, meiotic nuclei undergo dramatic chromosome reorganization upon meiotic entry that gives rise to their crescent-shaped

morphology visible by DAPI staining. Large aggregates or "patches" of nuclear envelope components are also present at this stage. We had previously speculated that PC ZnFs nucleate nuclear envelope patches since patches are always associated with a functional PC. Previous work in the lab showed that these large aggregates are essential for linking chromosomes to the cytoskeleton (Sato et al., 2009).

To look at the role PCs play in the formation of the meiotic bouquet, I performed immunofluorescence with antibodies against the nuclear envelope protein SUN-1. In *ieDf2* homozygotes, chromosomes remained uniformly dispersed within the nuclear volume as seen in premeiotic nuclei, and SUN-1 fails to aggregate at the nuclear envelope (Figure 1.2). These findings indicate that PCs are required to nucleate the aggregation of nuclear envelope components upon meiotic entry, and that these aggregates are essential for chromosome reorganization.

Pairing of homologous chromosomes is completely abrogated in the absence of Pairing Centers

The absence of an individual PC ZnF protein affects the pairing and synapsis of the cognate chromosome(s) (Phillips et al., 2005; Phillips and Dernburg, 2006). In various *him-8* mutants, the fraction of nuclei in pachytene with paired X chromosomes remain at levels similar to those observed in the premeiotic region, while the kinetics of Chromosome V homolog pairing is unaffected. The opposite effect is observed when pairing is assayed in the absence of ZIM-2, which binds chromosome V; chromosome V pairing levels remain similar to levels observed in the premeiotic region while pairing of the X chromosome is unaffected (Phillips and Dernburg, 2006). In other words, the defect in pairing and synapsis in single PC mutants are restricted to specific chromosomes.

Therefore we hypothesized that pairing is completely abrogated in the *ieDf2* mutant. To assay pairing, I performed fluorescent in situ hybridization (FISH) using probes against the PC and non-PC ends of chromosome V and the X chromosome (Figure 1.3A, data not shown). As expected, homolog pairing was completely abrogated. I divided a whole gonad into five zones of equal length and quantified the number of nuclei with paired FISH signals as a fraction of the total number of nuclei present in each zone (Figure 1.3B) For both chromosome V and the X chromosome, pairing levels at the PC and non-PC ends remained low and did not increase with meiotic progression.

Pairing Centers inhibit aberrant loading of SC components on chromosomes

In normal *C. elegans* meiosis, synapsis promptly follows homologous pairing. Although the mechanism of synapsis initiation is not well understood, the simple fact that we rarely, if ever, observe paired but unsynapsed chromosomes indicates that the initiation event is tightly linked to homolog pairing and that it happens relatively quickly. In fact, PCs have been implicated in synapsis initiation and shown to positively promote synapsis. Significantly more nuclei with fully

synapsed chromosomes are observed in a *meDf2* heterozygote, carrying a deletion of the X chromosome PC region, compared to a *meDf2* homozygote (MacQueen et al., 2005). Hence, it was possible that in the absence of homolog pairing and PC ZnFs, synapsis initiation would fail and chromosomes would remain unsynapsed throughout meiotic progression.

On the other hand, homolog pairing and synapsis in *C. elegans* are entirely separable events. A mutation in the highly conserved SUN domain of SUN-1 leads to extensive nonhomologous synapsis; chromosomes indiscriminately undergo synapsis with random partners (A. Penkner et al., 2007). Similar observations are observed in *sun-1* or *zyg-12(RNAi)* mutants, further highlighting the importance of proper chromosome-NE connections in homologous synapsis (Sato et al., 2009). Therefore we wondered whether chromosomes would undergo extensive nonhomologous synapsis in the *ieDf2* mutant, where proper connections to the nuclear envelope are essentially absent.

Immunofluorescence experiments with antibodies against components of the synaptonemal complex (SC), HTP-3 and SYP-1, revealed that the SC loads extensively in the *ieDf2* mutant regardless of global defects in pairing. HTP-3, an axial element component, loads on chromosomes immediately after cells enter meiosis and is part of the chromosome axes (Goodyer et al., 2008). In *ieDf2* mutants, HTP-3 loads on chromosomes with wild-type kinetics (Figure 1.4A).

SYP-1 is one of four known central element components of the SC and normally loads between chromosome axes (Colaiácovo et al., 2003; MacQueen et al., 2002; Smolikov et al., 2007; Smolikov et al., 2009). In the *ieDf2* mutant, SYP-1 loading remained limited in early meiotic nuclei except for 1-2 bright, thick linear aggregate(s) present in each nucleus. Analysis by FISH using probes against chromosome V and the X chromosome in separate experiments, revealed that these bright aggregates were not associated with a particular chromosome (data not shown). Though reminiscent of SC polycomplexes that arise in mutants defective in chromosome axes such as *htp-3(RNAi)* and *him-3(gk149),* I noted that the aggregates in *ieDf2* were more linear than globular and associated with chromosome axes ('early' inset, Figure 1.4A) (Couteau et al., 2004; Goodyer et al., 2008). The aggregates eventually disappear and SYP-1 loads more regularly in the region of the gonad corresponding to early pachytene ('mid' inset, Figure 1.4A). By late pachytene, SYP-1 was distributed completely along all chromosome axes ('late' inset, Figure 1.4A).

It was possible that aberrant loading of central components on chromosomes inhibited pairing in *ieDf2* mutants. To test this, I disrupted SC loading by knocking down SYP-2, a central element component, by RNAi in the *ieDf2* background. In *ieDf2; syp-2(RNAi)* mutants, pairing remains abrogated even in pachytene (Figure 1.4B).

Chromosomes undergo fold-over synapsis in the absence of PC activity

A closer look at pachytene nuclei in *ieDf2* mutants revealed the presence of 12 short, SC tracks per nucleus (Figure 1.5A). This is in stark contrast to the 6

long tracks of SC observed in wild-type, as well as in mutants that undergo extensive nonhomologous synapsis like *sun-1(jf18)*. This observation indicated that components of the SC were loading on individual, unpaired homologs. Because SYP-1 was fully associated with the chromosome axes, we reasoned that the SC may be polymerizing between sister chromatids instead of homologs, or that they may be loading between chromosomes that had folded-over.

Although synapsis between sister chromatids, or so called sister synapsis, has not been observed in *C. elegans*, the phenomena has been reported in other organisms. In budding yeast, the absence of cohesin-associated protein Pds5 results in the formation of an SC-like structure between sister chromatids, and meiotic chromosomes undergo hypercondensation (Jin et al., 2009). In vertebrates, a deletion of the meiotic cohesion complex component REC8 leads to sister synapsis although early pairing events seem normal (Xu et al., 2005).

Examples of SC loading between folded chromosomes, also called fold-over or self-synapsis, have been observed in many organisms including *C. elegans*. Chromosomes lacking a functional PC undergo fold-over synapsis when combined with a mutation in the crossover machinery (Rodenbusch, Thesis Research). Furthermore, in feminized *(fem-3*) males, the single X chromosome frequently undergoes self-synapsis, comparable to what has been observed in male XO mice (Jaramillo-Lambert & Engebrecht, 2010; Turner et al., 2005).

To differentiate between these two scenarios, I performed FISH using probes against the left and right arms of Chromosome V and simultaneously monitored SYP-1 loading by immunofluorescence. The two homologous signals are often far apart, and individual SCs associated with one signal for each probe are observed, reflecting fold-over synapsis in the *ieDf2* mutant (Figure 1.5B). Analagous experiments were performed using probes against the left and right arms of the X chromosome which yielded the same cytological pattern suggesting that all chromosomes undergo fold-over synapsis (data not shown).

Previous studies implicated the recombination machinery in promoting nonhomologous synapsis (Smolikov et al., 2008). Chromosomes aberrantly associate with SC central element components in *cra-1* mutants, which is abrogated by the introduction of *spo-11* or *mre-11,* genes required for double-strand break formation (Dernburg et al., 1998) and processing (Chin et al., 2001), respectively. In contrast, previous work in the lab showed that recombination inhibits fold-over synapsis of chromosomes lacking a functional PC (Rodenbusch, 2009). I investigated whether fold-over synapsis is dependent on double-strand breaks in *ieDf2* mutants by combining the *ieDf2* allele with a mutation in *mre-11*. My analysis indicated that the absence of double-strand breaks had no obvious effect on SC loading and *ieDf2; mre-11* mutants showed the same pattern of SC loading as single *ieDf2* mutants (data not shown).

Pairing Centers are required for the formation of crossovers but not double-strand breaks

The presence of a meiotic defect can be visualized by cytological analysis of diakinesis nuclei. At the end of meiotic prophase, the SC disassembles and chromosomes condense to give rise to six DAPI-staining bodies per nucleus, representing paired homologs that are linked together by chiasmata. Defects in pairing, synapsis or recombination ultimately lead to an increase in the number of DAPI-staining bodies at diakinesis. Thus this phenotype has been used as a visual read-out in screens for mutations affecting processes during meiotic prophase. Mutants defective in double-strand break formation like *spo-11(ok79)* result in nuclei at diakinesis containing twelve DAPI-staining bodies (Dernburg et al., 1998).

I quantified the number of DAPI-staining bodies in *ieDf2* mutants and discovered that over 75% of nuclei in diakinesis contained 11-12 DAPI staining bodies (Figure 1.6A). Variation in these numbers resulted from the resolution limits of our compound microscope. The presence of twelve univalents in *ieDf2* mutants indicated that crossovers were absent on all chromosomes. This was consistent with the observation that only 2.5% of embryos laid by *ieDf2* homozygotes were viable, a number comparable to that of *spo-11* mutants (Dernburg et al., 1998). And of the surviving adults, a significant percentage were males (Figure 1.6B). In these mutants, viable progeny arise from the rare occasion that a fertilized embryo receives a suitable complement of chromosomes sufficient for development. The Him phenotype is a result of X chromosome nondisjunction. In contrast, *ieDf2* heterozygotes do not exhibit these meiotic phenotypes, indicating that having only one copy of the four genes encoding PC ZnFs is sufficient for normal meiosis (Figure 1.6B).

To rule out the possibility that *ieDf2* mutants were defective in crossover formation due to their inability to form double-strand breaks, I performed immunofluorescence using an antibody against the RAD-51 protein, a highly conserved topoisomerase that catalyzes the strand-invasion reaction between homologous DNA molecules (reviewed in San Filippo, Sung, & Klein, 2008). In *C. elegans,* RAD-51 is visualized as foci on chromosomes in early pachytene and disappear by late pachytene, coincident with double-strand break repair (Alpi, Pasierbek, Gartner, & Loidl, 2003). In *ieDf2* mutants, RAD-51 foci were first observed in early pachytene, similar to wild-type, but remained at high levels until late pachytene (Figure 1.6C). Accumulation of RAD-51 foci can be attributed to the global defects in homolog pairing, and the absence of a homolog template required for double-strand break repair. Double-strand breaks are eventually repaired in *ieDf2*, presumably by using the sister chromatid as a template, based on the presence of discretely condensed DAPI-staining bodies later in diakinesis. In contrast, large masses of chromatin are observed in mutants that are defective in both homologous and sister recombination which are caused by DNA fragmentation and repair via non-homologous end joining (Hayashi et al., 2007).

Pairing Centers recruit PLK-2 to the nuclear envelope to facilitate phosphorylation of SUN-1

Concurrent studies on the meiotic role of *plk-2* by a fellow postdoc and graduate student in the lab, Sara Jover-Gil and Nicola Harper, respectively, lead to our further understanding of the function of PC ZnFs in early prophase. A yeast two-hybrid screen using a conserved domain of PLK-2 as bait identified HIM-8 as an interactor (Harper et al., 2011). Immunofluorescence experiments with an antibody against PLK-2 validated this result and revealed PLK-2's dynamic localization in the germline. Upon meiotic entry, PLK-2 colocalizes with PC ZnFs/SUN-1/ZYG-12 patches then later becomes increasingly associated with the SC in pachytene (Harper et al., 2011) .

We wondered whether PLK-2 recruitment to the nuclear envelope in early prophase is dependent on PC ZnF proteins. I monitored PLK-2 by immunofluorescence in the *ieDf2* mutant and discovered that in the absence of PC ZnFs, PLK-2 does not localize to the nuclear envelope but remains associated with the SC, including the bright aggregates previously described in early prophase (Figure 1.7A). This result suggests that PC ZnFs recruit PLK-2 to NE patches during early prophase. Consistent with this idea, PLK-2 remains associated with PC ZnFs at the nuclear periphery in the absence of proper NE patches in *gk199* mutants, a null allele of *sun-1* (Harper et al., 2011).

We further speculated that function of PLK-2 at patches may depend on its kinase activity. Reorganization of SUN-1/ZYG-12 at the nuclear envelope of early prophase nuclei are dependent on specific post-translational modifications of SUN-1 (Penkner et al., 2009). Upon meiotic entry, a series of serine residues become phosphorylated, including Ser8 and Ser12. While Ser8-Pi is detected all over the nuclear envelope, Ser12-Pi is restricted at patches. Both phosphorylation events are dependent on *chk-2*, an important regulator of early meiotic prophase events, though it is not known whether CHK-2 directly phosphorylates these residues (MacQueen et al., 2001; Penkner et al., 2009).

Because of the striking similarity observed between PLK-2 localization and the pattern of Ser12-Pi, we wondered whether phosphorylation of Ser12 is dependent on PLK-2. To test this hypothesis, I used phospho-specific antibodies against both Ser8-Pi and Ser12-Pi in the *ieDf2* mutant, where PLK-2 fails to localize to the nuclear envelope (Figure 1.7B). While Ser8 phosphorylation was intact in the absence of PC ZnF proteins, Ser12 phosphorylation was completely abrogated. These results suggest a specific role for PLK-2 in phosphorylating Ser12. Consistent with this idea, Ser12 phosphorylation is relatively weaker in a *plk-2* mutant compared to wild-type and completely abrogated in a *plk-2*; *plk-1 (RNAi)* double mutant. In the absence of PLK-2, PLK-1 is recruited to NE patches where it can partially substitute for PLK-2 function, yet is not sufficient due to the meiotic defects observed in *plk-2* mutants (Harper et al., 2011). Taken together, our collaborative research elucidates the function of PC ZnFs in recruiting PLK-2 to the nuclear envelope to facilitate the phosphorylation and reorganization of SUN-1.

A conserved Polo-box binding motif in HIM-8 is required for its interaction with PLK-2

The conserved Polo box domain (PBD) found in PLKs often determines substrate specificity by binding a phosphothreonine or phosphoserine, usually in the context of S-pS/T-P, of its substrates or associated proteins. A closer look at the primary sequences of PC ZnF proteins uncovered the presence of a putative Polo box binding motif at their N-terminal regions (Figure 1.8A). However, whether the PBD-binding motif is functionally relevant to PLK-2 or PC function remained to be addressed.

The *him-8(me4)* allele is a missense mutation immediately downstream of the PBD-binding motif. In this mutant, HIM-8(S85F) is expressed and localizes to the X chromosome PC and the nuclear periphery, but fails to associate with a SUN-1/ZYG-12 patch (Sato et al., 2009)). Accordingly, the X chromosome fails to pair and synapse (Phillips et al., 2005). We found that PLK-2 is not recruited to the unpaired HIM-8(S85F) foci, indicating that the region of HIM-8 including the mutated residue is important for its interaction with PLK-2 (Figure 1.8C). Furthermore, it suggests that PC function requires PLK-2 activity.

To address whether the PBD-binding motif is essential for PLK-2's interaction with PC ZnFs and its recruitment to the nuclear envelope, I utilized a combination of the yeast two-hybrid system and *in vivo* transgenic techniques. Using the PBD fragment as bait, I carried out pairwise yeast two-hybrid assays with various fragments of HIM-8 and found that a minimal fragment of 112 amino acids was sufficient for its interaction with PLK-2 (Figure 1.8B). This fragment contains the PBD-binding motif as well as the region immediately downstream surrounding the site of the *him-8(me4)* allele. Smaller fragments containing the PBD-binding motif alone (aa 41-80) or the region downstream which lacks the PBD-binding motif (aa 70-112) failed to interact with PLK-2 in this assay, suggesting that both regions may be required for proper interaction between HIM-8 and PLK-2. While the PBD-binding motif is not sufficient for interaction with HIM-8, I show that it is necessary by introducing a mutation within the PBD-binding motif. Changing threonine 64 to an alanine abolished the interaction between HIM-8 and PLK-2. I also found that HIM-8(S85F) does not interact with PLK-2 in the yeast two-hybrid assay, which is consistent with the observation that PLK-2 does not associate with HIM-8(S85F) *in vivo.*

To test whether the PBD-binding motif in HIM-8 is required for PLK-2 interaction and recruitment to the nuclear envelope *in vivo*, I created transgenic lines carrying single-copy insertions of the wild-type *him-8* gene or an allele expressing the mutant protein HIM-8(T64A). Both transgenes were crossed to *him-8(tm611),* a deletion allele that abrogates binding of HIM-8 to the X chromosome PC (Phillips et al., 2005). The wild-type transgene fully complemented *him-8(tm611)* and HIM-8 foci formed at the nuclear envelope and colocalized with PLK-2 (Figure 1.8D). In contrast, expression of HIM-8(T64A) failed to rescue the Him phenotype. Unpaired HIM-8(T64A) foci localized to X

chromosome PCs and the nuclear periphery but remained unassociated with PLK-2, a phenotype similar to HIM-8(S85F) (Figure 1.8E).

Functional PCs are required for the activation of the synapsis checkpoint in meiotic prophase

In *C. elegans,* two separate and distinct checkpoints exist in the germline to ensure accurate meiotic segregation (Bhalla & Dernburg, 2005; Colaiácovo et al., 2003; MacQueen et al., 2002). Unsynapsed chromosomes can trigger the selective apoptosis of the affected oocyte near the end of meiotic prophase. It was previously shown that this checkpoint requires the presence of an unsynapsed, functional PC bound by its cognate ZnF. The DNA damage checkpoint is triggered by the presence of unresolved breaks, independent of synapsis, and similarly results in apoptosis.

I predicted that in the *ieDf2* mutant which lacks all PC ZnFs, unsynapsed chromosomes would fail to trigger the synapsis checkpoint. To monitor apoptosis, I counted the number of corpses in late pachytene by methods previously described using a strain expressing *ced-1::gfp* (Schumacher et al., 2005). I found elevated levels of apoptosis in *ieDf2* mutants as expected, due to both the presence of unsynapsed chromosomes and persistent, unresolved DSBs. I introduced a mutation in *pch-2,* a gene required for the synapsis checkpoint (Bhalla & Dernburg, 2005), to look at its effect in apoptosis. As predicted, *ieDf2; pch-2(tm1458)* animals display the same increased levels of apoptosis as *ieDf2* mutants, indicating that the synapsis checkpoint does not contribute to the increased levels. To confirm that the observed increase in apoptosis was due to the DNA damage checkpoint, I crossed *ieDf2* to *hus-1(op241).* I found that *ieDf2; hus-1* animals displayed wild-type levels of apoptosis, indicating that the increase in apoptosis was caused by the DNA damage checkpoint. These results are consistent with prior evidence that the synapsis checkpoint pathway requires functional PC ZnFs (Bhalla & Dernburg, 2005).

Concluding Remarks

PC ZnFs recruit PLKs to the nuclear periphery

A fundamental question addressed in this study is how chromosome attachment and clustering at the nuclear envelope is regulated to ensure proper chromosome dynamics during meiosis. It was previously shown that PCs associate with aggregates of transmembrane proteins that bridge the nuclear envelope to connect chromosomes to the cytoskeleton (Sato et al., 2009). These connections are essential to coordinate pairing and synapsis so that the SC forms only between properly paired homologs. By engineering and analyzing a PC-null mutant, I show that PC ZnFs are required for the recruitment of a polo-like kinase PLK-2 to the nuclear envelope where it is required for the phosphorylation of SUN-1 at Ser12 and the reorganization of NE components to establish proper connections to the cytoskeleton.

Localization of PLK-2 to the nuclear periphery and phosphorylation of SUN-1 at Ser12 is not, however, sufficient for its reorganization. Labella et al. (2011) showed that in a *sun-1(jf18)* mutant, PLK-2 is recruited by PC ZnFs, SUN-1 at Ser12 is phosphorylated, but patches do not form, indicating that other factors such as proper interactions with ZYG-12 and the cytoskeleton, in addition to SUN-1 phosphorylation, are required to promote reorganization of these complexes at the nuclear envelope.

It is interesting to note that while HIM-8 was identified as a Y2H interactor of PLK-2 from a screen using both the full-length sequence and the PBD alone as bait (Harper et al., 2011), none of the ZIM proteins were identified. Furthermore, interaction between ZIM-3 and PLK-2 PBD was tested in a Y2H pairwise assay and yielded negative results (data not shown). Polo-like kinases often interact with proteins that contain a PBD binding motif like that found in HIM-8 and the ZIM proteins and the interaction is often dependent on a priming kinase which phosphorylates the serine or threonine within the sequence. It is possible that HIM-8 which is somewhat diverged from the other ZIM proteins (Phillips and Dernburg, 2006) is more readily primed by a yeast kinase.

How phosphorylation of SUN-1 at Ser12 promotes patch formation is not clearly understood. One hypothesis is that SUN-1 may be constrained by its association with other proteins or the lamina at the nuclear periphery and phosphorylation of SUN-1 affects its ability to bind to these factors thereby releasing these constraints. It is also possible that PLK-2 phosphorylates additional proteins at the nuclear periphery that can induce changes in the mobility of SUN-1. By identifying PLK-2 substrates, we can begin to address these remaining issues.

An additional question addressed by analyzing the PC-null mutant

The *ieDf2* deletion allele allowed me to address another interesting question regarding the role of PC ZnFs in meiotic progression. It was possible that PC ZnFs had additional and redundant roles during meiosis that could not be elucidated by analysis of single mutants. In particular, we wondered whether expression of PC ZnFs were required for entry into meiosis. This was clearly not the case; meiosis-specific proteins like HTP-3 and SYP-1 were expressed and loaded readily on chromosomes. In addition, SUN-1 Ser8 was phosphorylated in *ieDf2* mutants, a mark that is restricted to meiotic cells in early prophase (Penkner et al., 2009).

Materials and Methods

C. elegans strains, genetics, and culture conditions

Unless otherwise stated, all animals were cultured under standard conditions at 20˚C (Brenner, 1974) . The wild-type strain was N2 Bristol. The *ieDf2* deletion allele was constructed by MosDel (Frøkjaer-Jensen et al., 2010). The

ttTi22866 Mos1 insertion strain was provided by the Ségalat lab and the The presence of the expected *Mos1* element to the right of *him-8* was confirmed by PCR, and crossed to *unc-119(ed3)* to create strain CA870. A donor template was constructed by inserting a 2.6-kb genomic fragment immediately to the right of the *Mos1* insertion and a 3-kb genomic fragment immediately to the left of the *zim-1* coding region into pRL8 (gifted by Christian Frokjaer-Jensen, Jorgensen Lab), flanking the *C. briggsae unc-119*$^{+}$ rescuing fragment. This was coinjected into CA870 hermaphrodites with pJL43.1, pGH8, pCFJ90 and pCFJ104, as described (Frokjaer-Jensen et al., 2010). Non-Unc, mCherry-minus progeny were identified after several generations. Successful excision of the expected 20-kb genomic segment was verified by PCR, outcrossed 3 times to *unc-119(ed3)*, and maintained over *mIs11*. Loss of HIM-8 and ZIM protein expression in deletion homozygotes was verified by immunofluorescence.

Single-copy insertions of wild-type *him-8* and *him-8*(T64A) were generated by MosSCI (Frøkjaer-Jensen et al., 2008). The *him-8* genomic sequence, including 943 bp upstream and 615 bp downstream of the coding region, was inserted into pCFJ151 to generate a donor template (pREG52). Site-directed mutagenesis was performed to generate the T64A allele, which was verified by sequencing. EG4322 animals were injected with either wild-type or mutant donor template, pJL43.1, pGH8, pCFJ90, and pCFJ104. Homozygous insertions (*ieSi13* and *ieSi14*) were confirmed by PCR, crossed into *him-8(tm611)* and assayed for rescue of the Him phenotype and expression of HIM-8 by immunofluorescence.

Yeast two-hybrid assays

Pair-wise yeast two-hybrid assays were performed using the ProQuest™ Two-Hybrid System (Invitrogen). The PLK-2 C-terminal domain containing amino acids 280-632, which spans the Polo box domain but not the kinase domain, was amplified from a cDNA library, sequence-verified, and cloned into bait vector pDEST32. Absence of self-activation was tested before pair-wise assays.

Full-length coding sequences of HIM-8 and ZIM-3 were amplified from a cDNA library, sequence-verified, and cloned into prey vector pDEST22. The resulting HIM-8 prey vector was used as a template for site-directed mutagenesis to generate the T64A and S85F mutations. Expression of the mutant proteins was verified by Western blotting. Various fragments of the HIM-8 coding sequence (Figure 1.9) were also cloned into the same prey vector.

Cytological methods

Immunofluorescence was performed as previously described (Phillips et al., 2009a). Young adult hermpahrodites were dissected in egg buffer containing sodium azide and .1% Tween-20, fixed for 2-3 minutes in egg buffer+1% formaldehyde between a Histobond slide and coverslip, and frozen on dry ice. The coverslip was removed and slides were transferred to -20˚C methanol for 1 minute. Slides were transferred to PBST(containing .1% Tween-20), washed in 2 further changes of PBST, blocked with Roche blocking agent for 20 minutes, and

stained with primary antibodies for 2 hours at room temperature or overnight at 4˚C. Following 3 consecutive washes with PBST, slides were stained with secondary antibodies labeled with Alexa 488, Cy3 or Cy5 for 1-2 hours at room temperature. Slides were washed with 3 consecutive times in PBST, with the second wash containing .5ug/ml DAPI to stain chromosomes, and mounted in glycerol-based mounting medium containing n-propyl gallate.

Fluorescence in situ hybridization (FISH) procedures have also been previously described in detail (Phillips et al., 2009a). Probes used in this study included the 5s rDNA repeat (A F Dernburg et al., 1998), a short repeated associated with the right end of the X chromosome (Phillips et al., 2005), and single-copy probes to the left end of chromosome V (MacQueen et al., 2005)and the left arm of the X chromosome (Phillips et al., 2005).

Apoptosis in mutant strains was quantified by introduction of the *bcIs39* (Plim-7::ced-1::gfp) reporter construct (Schumacher et al., 2005). Live animals were mounted on agarose pads and evaluated using a compound objective. Germline nuclei that are completely surrounded by green fluorescence were counted as previously described (Bhalla & Dernburg, 2005).

Images were acquired using a DeltaVision RT system (Applied Precision) equipped with a 100x N.A. 1.40 oil-immersion objective (Olympus), resulting in an effective XY pixel spacing of 0.067 or 0.045 μm. 3D image stacks were collected at .2μm Z-spacing and processed by constrained, iterative deconvolution. Image scaling and analysis were performed using functions in the softWorx software package. Projections were calculated by a maximum intensity algorithm. Composite images were assembled and false colorizing performed with Adobe Photoshop.

Quantification of chromosome pairing

Pairing at the PC and non-PC regions of Chromosome X and V were measured in gonads marked by FISH. 3D images of germline nuclei were divided into five zones of equal length and pairing was scored as the fraction of nuclei in each zone with paired FISH signals. Separate experiments were performed for each chromosome. Three whole gonads were analyzed per genotype.

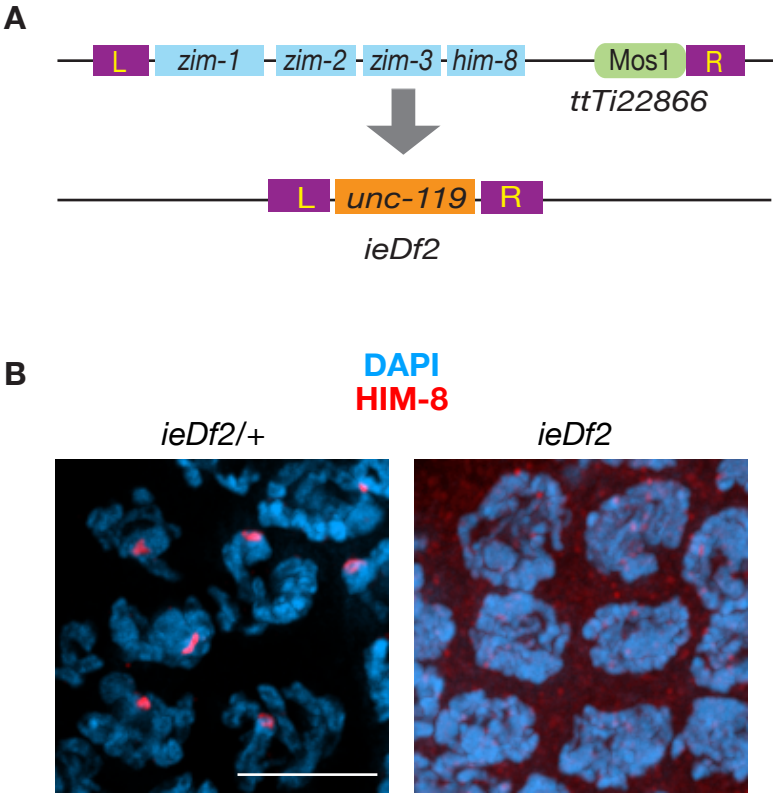

Figure 1.1 Targeted deletion of *zim-1, zim-2, zim-3* and *him-8*. (A) A 20-kb genomic region on Chromosome IV was deleted by a transposon-based deletion technique *MosDel* resulting in the *ieDf2* allele. (B) An antibody against HIM-8 was used to detect its expression in *ieDf2/+* and *ieDf2* animals. Signal is intensified in the *ieDf2* image to show absence of weak expression. Scale bar, 5μm.

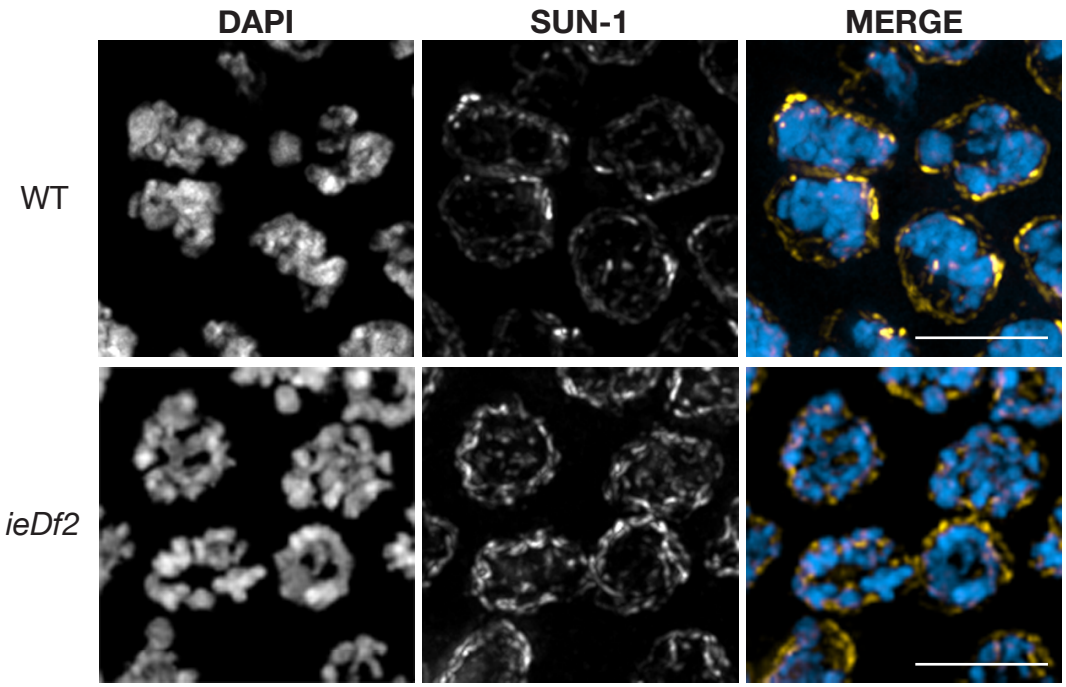

Figure 1.2 Hallmarks of early meiotic nuclei are absent in PC-null animals. Images are maximum-intensity projections of 3D stacks of meiotic nuclei in early prophase. Chromosome clustering and SUN-1 aggregates are absent in *ieDf2* mutants. Scale bar, 5μm.

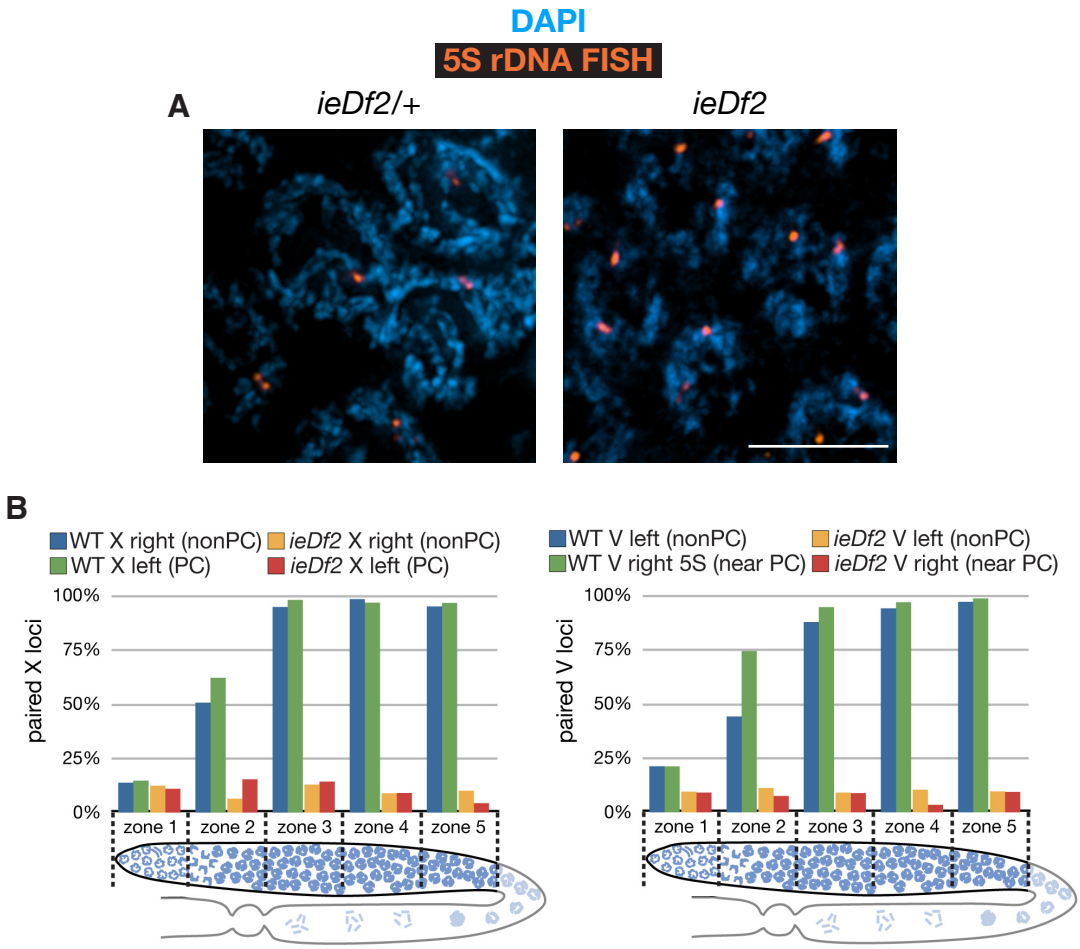

Figure 1.3 Homologous pairing is completely abrogated in *ieDf2* mutants. (A) Chromosome V is labeled by FISH using the 5s rDNA probe. A field of pachytene nuclei from an *ieDf2* heterozygote shows paired signals while pairing is absent in the *ieDf2* homozygote. (B) PC and non-PC ends of Chromosome V and the X Chromosome were labeled by FISH. 3D images of whole gonads were divided into five zones of equal length. The fraction of nuclei with paired FISH signals were counted in each zone. Percentages represent the average of 3 whole gonads of each genotype. Percent of nuclei with paired homologs in *ieDf2* homozygotes remain similar to those observed in premeiotic nuclei (zone 1) and fail to increase with meiotic progression. Scale bar, 5μm.

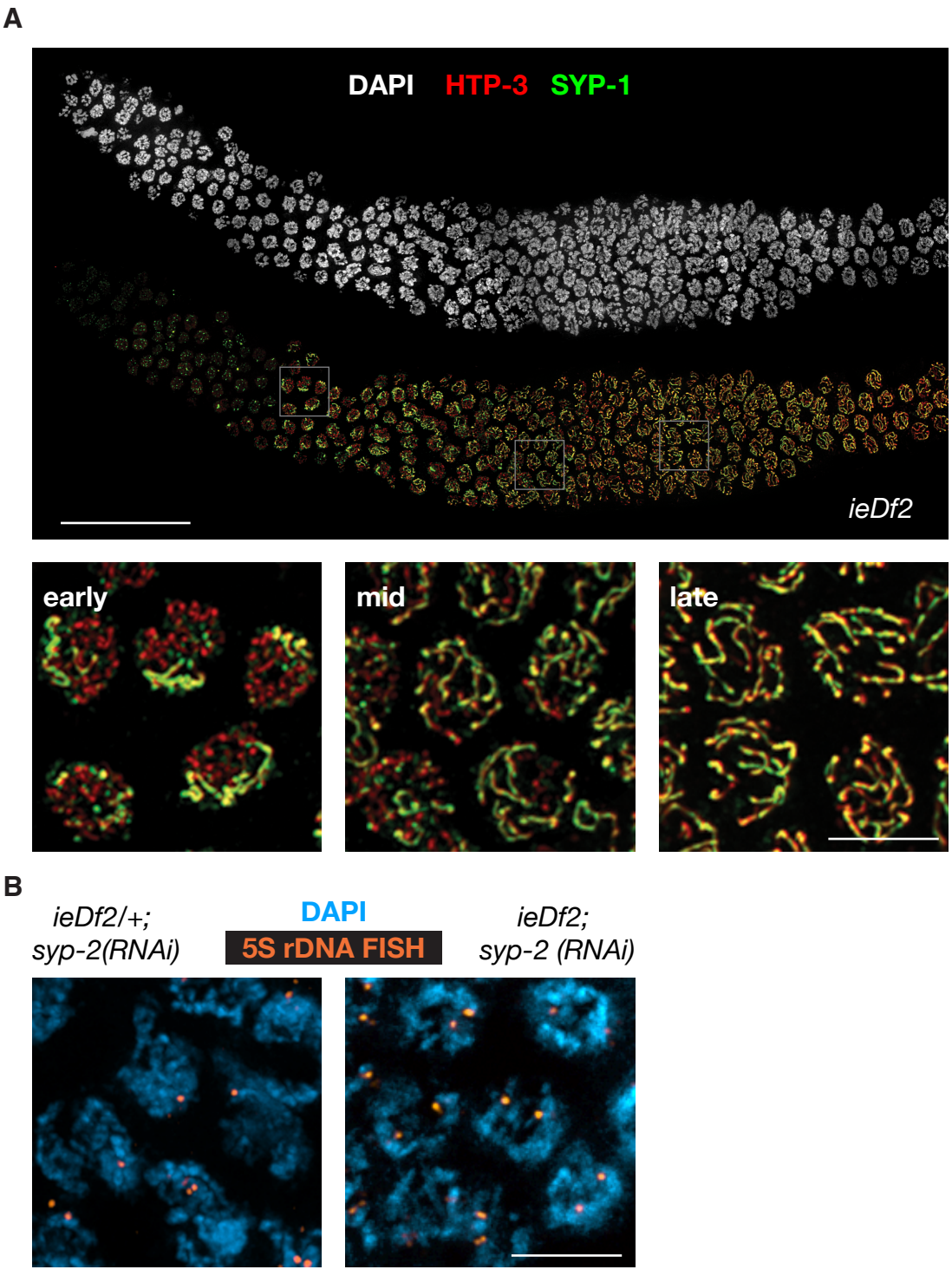

Figure 1.4 Extensive loading of SC components in the absence of PCs. (A) Chromosome axes are detected in early prophase, but central region components of the SC load aberrantly in *ieDf2* hermaphrodites. Composite projection images of gonads from wild-type and *ieDf2* animals, stained with DAPI (grayscale), anti-

HTP-3 (axial element protein, red), and anti-SYP-1 (central region protein, green). Meiotic progression is from left to right. Scale bar, 30µm. The panel on the bottom shows higher-magnification images of early (transition zone region), mid (early pachytene) and late (late pachytene) prophase nuclei. In early prophase, brightly staining SYP-1-containing structures are associated with a subset of chromosomes. *ieDf2* shows extensive loading of SC (marked by SYP-1) by late pachytene. Scale bar, 5µm. (B) Failure of homologous pairing in *ieDf2* hermaphrodites in the absence of synapsis. Hybridization to the 5S rDNA locus is shown in orange. Scale bar, 5µm.

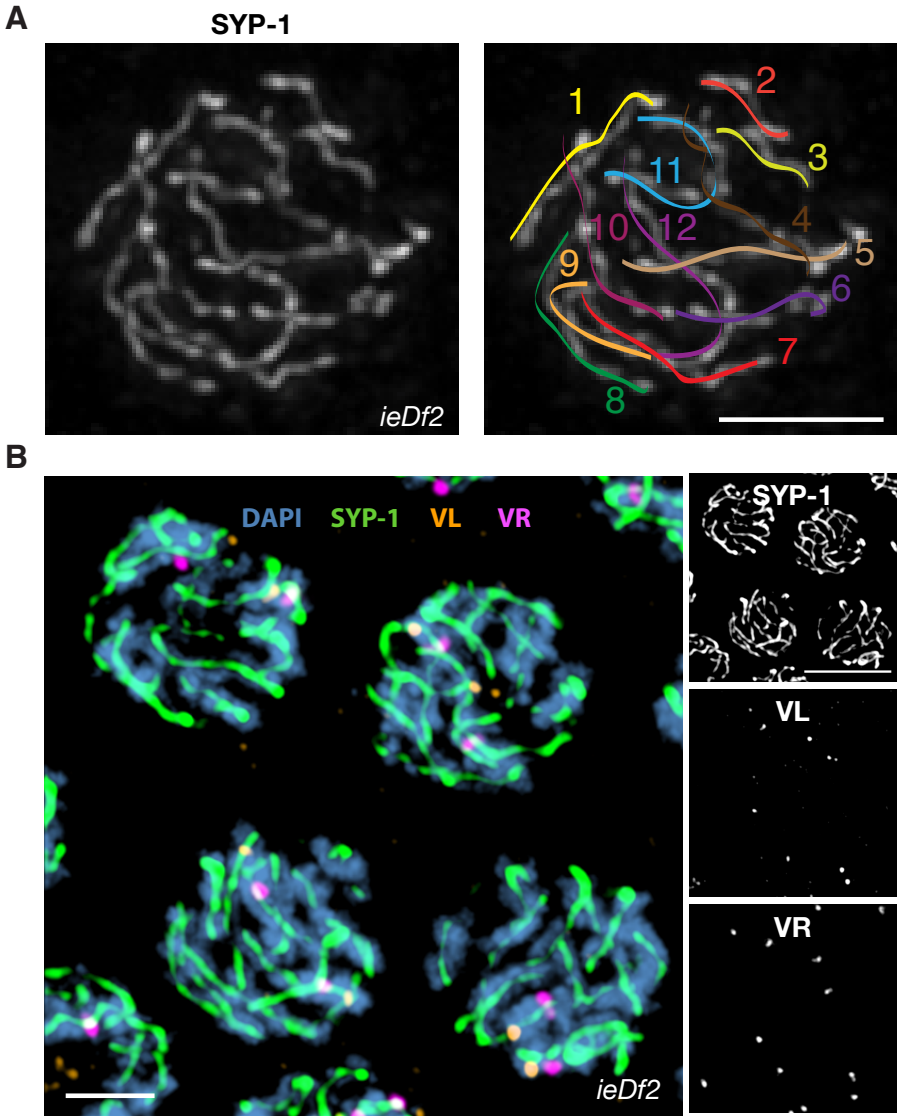

Figure 1.5 Chromosomes undergo fold-over synapsis in the absence of PCs. Evidence that synaptonemal complex formation in *ieDf2* hermaphrodites occurs between nonhomologous regions of individual chromosomes. (A) Pachytene nuclei in *ieDf2* homozygotes contain 12 short stretches of SC, rather than 6 longer SCs. *Left:* Projection image of a representative nucleus stained with anti-SYP-1. *Right:* Tracing of contiguous SYP-1 tracks through the 3D data stack reveals 12 discrete segments, consistent with fold-back synapsis of each chromosome. Scale bar, 2μm. (B) Projection images of representative pachytene-stage nuclei of the indicated genotypes, stained with SYP-1 antibodies (green) and hybridized with fluorescent probes marking loci near the left end (orange) and the right arm (5S rDNA locus; pink) on Chromosome V. In the *ieDf2* mutant, SC loads between folded chromosomes. Scale bar, 2μm (higher magnification image) and 5μm (lower magnification images).

A

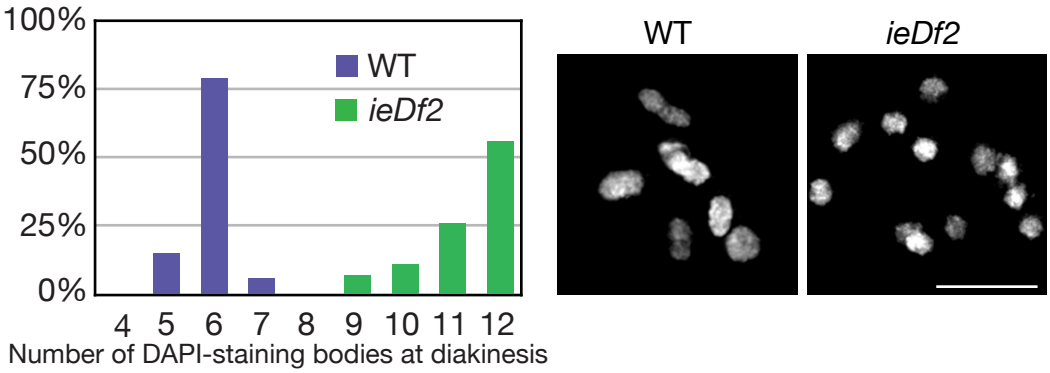

B

genotype	% males (# of adults scored)	% viable embryos (# of embryos scored)
wild-type	.1 (3280)	108.0 (3035)
ieDf2/+	.3 (2067)	100.9 (2047)
ieDf2	17.1 (36)	2.5 (1418)

C

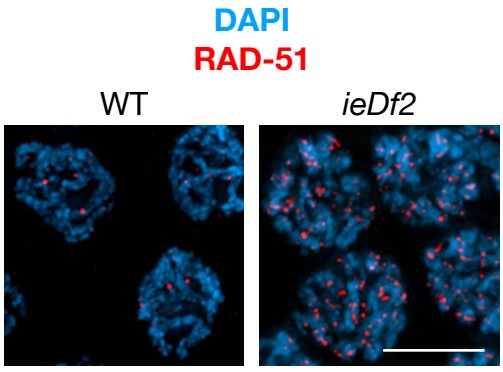

Figure 1.6 PCs are required for the formation of crossovers but not double-strand breaks (A) Quantification of DAPI-staining bodies at diakinesis in wild-type and *ieDf2* hermaphrodites. 100 oocytes were scored for each genotype. The variation in reported numbers for WT and *ieDf2* oocytes is a consequence of the resolution limit of the microscope; other data indicate that there are no crossovers in the mutant. Representative projection images are shown to the right. Scale bars, 5µm.(B) The fraction of viable embryos and adult male progeny were quantified in whole broods of self-fertilized hermaphrodites. The numbers of adults or embryos counted are indicated in parentheses. Apparent viability of >100% is a consequence of missing some embryos. (C) PCs are not required for DSB formation. RAD-51 foci are much more abundant in late pachytene oocytes from *ieDf2* than from wild-type hermaphrodites, due to delayed repair in the absence of homolog pairing. Scale bar, 5µm.

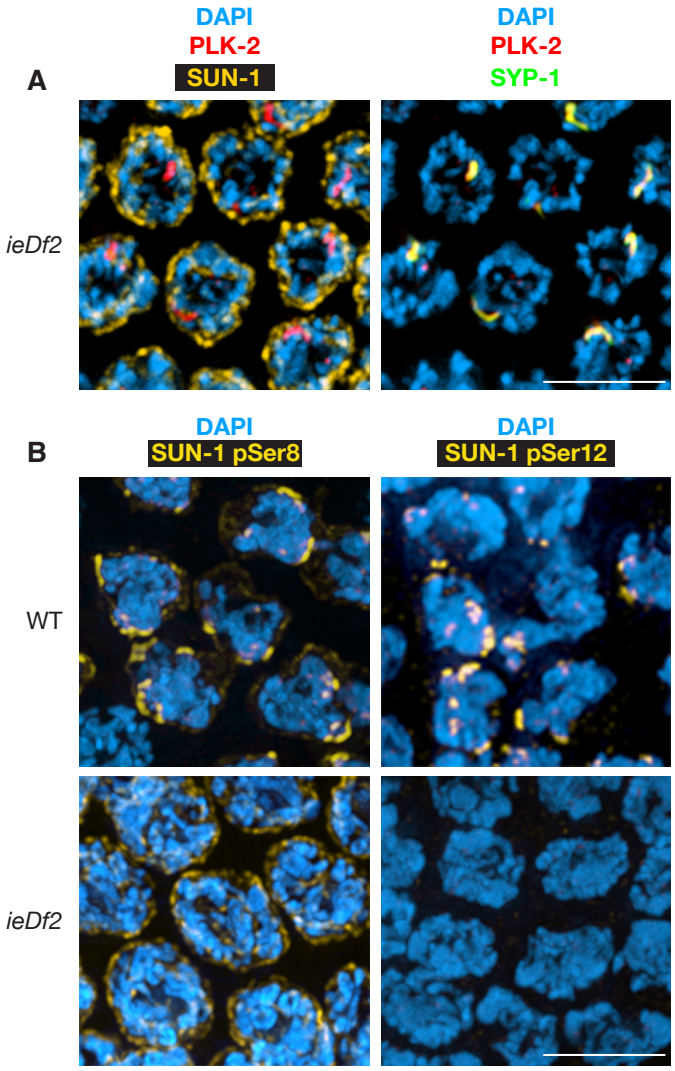

Figure 1.7 PCs recruit PLK-2 to the nuclear envelope to facilitate specific phosphorylation of SUN-1. (A) In *ieDf2* mutants, PLK-2 (red) colocalizes with SC central region protein SYP-1 (green) in early prophase, but not with SUN-1 (yellow). (B) Immunofluorescence using antibodies against SUN-1 phosphoepitopes reveals that phosphorylation at Ser12, but not at Ser8, depends on PC function. Scale bar, 5µm.

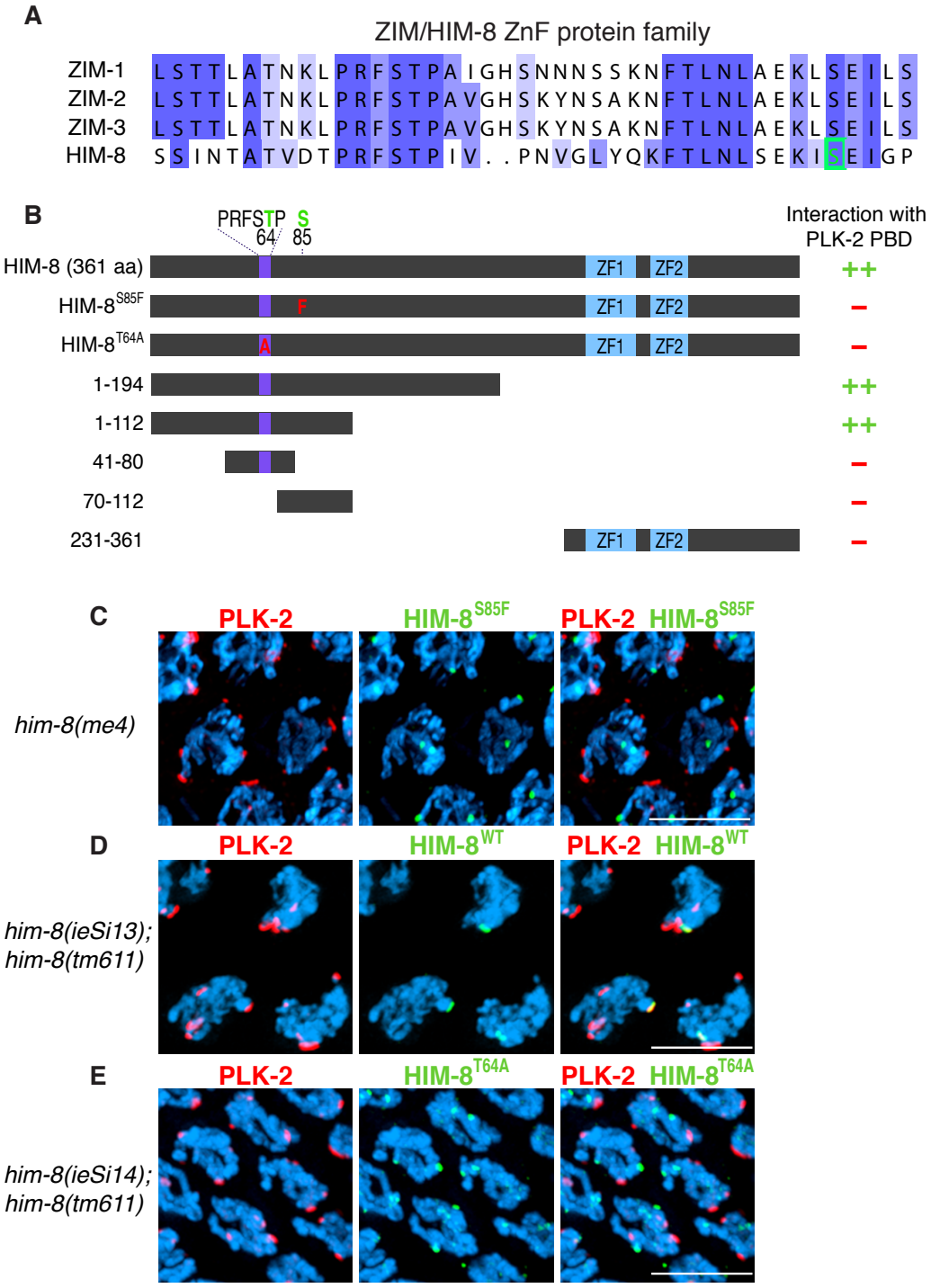

Figure 1.8 HIM-8 interacts with the Polo box domain (PBD) of PLK-2. (A) All four ZnF proteins in *C. elegans* contain one or two copies of a short, highly conserved amino acid sequence (PRFSTP) containing a potential PBD-binding site. It is unknown whether the Thr in the PRFSTP sequences is phosphorylated.

An adjacent, more loosely conserved motif within the proteins contains an invariant serine residue. The *him-8(me4)* allele is a mutation of this invariant serine (highlighted in green) to phenylalanine. **(B)** Summary of pairwise yeast two-hybrid interactions between the PBD of PLK-2 and the indicated HIM-8 fragments or mutants. Full-length HIM-8 is 361 amino acids. The position of threonine 64 is indicated, and the PRFSTP motif that contains this residue and is conserved among all PC ZnF proteins is indicated in purple. Serine 85 is also indicated. Amino acid changes in two of the constructs (S85F and T64A) are highlighted in red. The two zinc finger domains, ZF1 and ZF2, are indicated in blue. **(C)** HIM-8^{S85F}, encoded by *him-8(me4)*, binds to the X chromosome PCs, but is unable to recruit PLK-2 or to promote X chromosome pairing (see also Phillips *et al.*, 2005). **(D)** Hermaphrodites carrying a transgene (*ieSi13*) encoding wild-type HIM-8 show paired HIM-8 foci that are associated with PLK-2. **(E)** Meiotic nuclei in hermaphrodites carrying a transgene (*ieSi14*) encoding HIM-8^{T64A} show unpaired HIM-8 foci that lack PLK-2 staining.

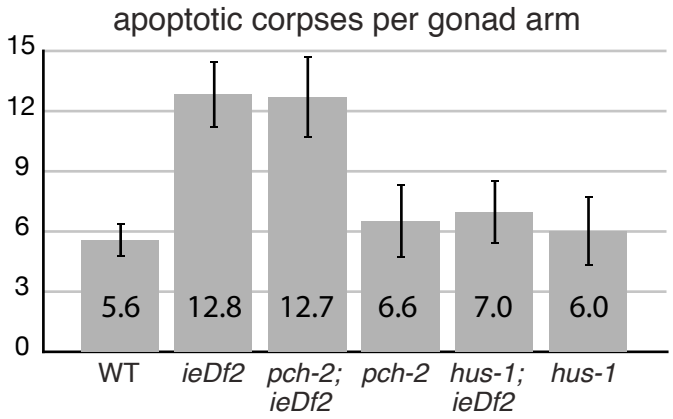

Figure 1.9 PCs are required for the activation of the synapsis checkpoint but not the DNA damage checkpoint. *ieDf2* mutants show elevated apoptosis that depends on the DNA damage checkpoint, but not the synapsis checkpoint. Germline apoptosis in animals of the indicated genotypes was quantified using CED-1:GFP fluorescence, as described in the Materials and Methods. Loss of *pch-2*, which disrupts the synapsis checkpoint (Bhalla and Dernburg, 2005), does not reduce germline apoptosis in *ieDf2* homozygotes. However, when the DNA damage checkpoint is abrogated by introduction of *hus-1(op241)*, only baseline, or "physiological" apoptosis is observed. At least 22 gonads were scored for each genotype. Error bars represent the standard error of the mean.

Chapter 2: Candidate screen for meiotic regulators of chromosome dynamics

Summary

As described in the previous chapter, attachment of chromosomes to nuclear envelope SUN/KASH bridges via PC ZnF proteins are essential for proper meiotic chromosome dynamics. How nuclear envelope proteins contribute to homology assessment is not well understood. To address this, I aimed to identify novel regulators of meiotic chromosome dynamics through a candidate screen, and I will present my preliminary characterization of their meiotic defects in this chapter. I focused my analysis on one of these mutants, *spd-3,* which was previously cloned. In addition, I will describe tools that I generated for imaging of chromosome dynamics in living worms.

Introduction

Meiotic chromosome dynamics play a vital role in proper homolog pairing and synapsis in *C. elegans*. In the previous chapter, I described how chromosomes, bound by a family of zinc finger proteins, recruit a kinase to the nuclear envelope, which is required to establish proper connections between chromosomes and the cytoskeleton. In the work described in this chapter, my goals were to identify novel regulators of meiotic chromosome dynamics and to construct tools that would enable visualization of these dynamics *in vivo.*

Many of the components that are now known to be required for meiotic chromosome dynamics play additional, essential roles in mitosis. SUN-1 and ZYG-12 are required for the attachment of centrosomes to the nuclear envelope during early embryogenesis (Malone et al., 2003). In *zyg-12* mutants, centrosomes detach from the nuclear envelope of the paternal pronucleus after fertilization, resulting in misaligned mitotic spindles in 1-cell embryos. SUN-1 is required for recruitment of ZYG-12 to the outer nuclear membrane, and therefore plays an essential role in this process as well. Cytoplasmic dynein contributes to diverse processes in early embryogenesis, including centrosome rotation, pronuclear migration, bipolar spindle assembly, anaphase chromosome segregation and cytokinesis (Gönczy et al., 1999; Schmidt et al., 2005).

Due to their various roles in mitosis, strong loss-of-function alleles of *sun-1, zyg-12, dhc-1,* or *dlc-1* lead to a failure in germline proliferation and sterility. Homozygous mutant animals from heterozygous mothers that carry deletion alleles of *sun-1(gk199)* or *zyg-12(ie14)* develop into adults due to maternal contribution (Penkner et al., 2007; Sato et al., 2009). However, these mutant animals develop disorganized mitotic germlines with polyploid nuclei that fail to complete meiosis. Weaker, hypomorphic alleles, on the other hand, reveal these genes' specific functions in homolog pairing and synapsis during meiotic prophase (Malone et al., 2003; Penkner et al., 2007; Sato et al., 2009). Based on this observation, we postulated that additional, unknown components that function with SUN-1/ZYG-12 patches to coordinate pairing and synapsis may exhibit a similar phenotypic pattern. We predicted that loss-of-function alleles in such factors would also lead to a sterile phenotype.

In an effort to identify novel components of the cell-division machinery, O'Connell et al. (1998) carried out a screen. The screen was designed to yield temperature-sensitive mutations in genes affecting various aspects of cell division, independent of developmental age and cell type. They looked for mutants that displayed the "sterile and uncoordinated" (Stu) phenotype, which reflects defects in the cell divisions essential for the proliferation of the germline and motor neurons, respectively. A large number of mutants were recovered in a screen of 55,000 haploid genomes. Subsequent analyses revealed specific roles in early embryogenesis for a subset of these mutants (e.g., cytokinesis, chromosome segregation, spindle positioning, centrosome morphology, etc.), but their potential

roles in meiosis had not been investigated. Here, I present data revealing some of the mutants recovered display meiotic defects at the non-permissive temperature. I also describe tools I generated to visualize chromosome dynamics *in vivo.*

Results and Discussion

Candidate screen for novel regulators of meiotic chromosome dynamics

A preliminary screen of candidate mutants was performed by shifting the animals to the non-permissive temperature, 25˚C, at the L4 stage for 48 hours. By the L4 stage, the germline has proliferated extensively, and many nuclei have entered meiosis. The first of these nuclei are destined to become spermatocytes, but the switch to oogenesis normally occurs at the onset of adulthood. After 48 hours, I dissected gonads from the mutant animals and performed immunofluorescence with a combination of antibodies (α-HIM-8, α-SYP-1, and α-SUN-1) that allowed me to visually screen for a range of meiotic defects, including failures of homolog pairing or synapsis.

To assay pairing, I used an antibody against the HIM-8 protein, which binds to the pairing center region of the X chromosome. Synapsis defects were detected by visualizing SYP-1, a component of the transverse filaments of the SC. A global defect in synapsis would lead to the loss of SYP-1 tracks in pachytene and/or the presence of large SC polycomplexes, which arise when the SC cannot load on chromosome axes (reviewed in Zickler & Kleckner, 1999). More subtle defects in synapsis, which may result in a few unsynapsed chromosomes, would not be readily obvious by looking at SYP-1 staining alone. However, such defects can be assayed by the presence of an extended early prophase region, characterized by the persistence of SUN-1 patches.

Among the 18 candidate mutants screened, several displayed meiotic defects: *stu-9*, *stu-10, stu-11, stu-13, stu-15*, and *spd-3*. Two of the mutants, *abc-1* and *cyk-2,* had severe polyploidy that made it difficult to assess pairing and synapsis accurately. A complete list of mutants and results from the preliminary screen are presented in Table 1.

stu-10, stu-11*, and* stu-13 *display synapsis defects*

Preliminary analysis revealed a subset of mutants with synapsis defects: *stu-10, stu-11,* and *stu-13*. Since candidate mutants were originally derived from a screen for general cell-division machinery components, it was not surprising to discover that some mutants, such as *stu-10* and *stu-13*, also exhibited mitotic defects in the germline, giving rise to polyploid cells undergoing meiosis. This made it difficult to assess meiotic defects due to the varying number of chromosomes per nucleus, which affects the number of HIM-8 foci present. Moreover, the presence of extra chromosomes would potentially affect synapsis indirectly, since some chromosomes might lack a homologous partner. To further analyze meiotic defects while minimizing mitotic defects, I shifted *stu-10* and *stu-13* animals for 24 hours instead of 48 hours. Although this shorter temperature shift produced far fewer polypoid cells in the germline, an extended transition zone and unsynapsed chromosomes were still observed in *stu-10* and *stu-13* mutants (Figures 2.1A, 2.3B, data not shown). RNAi of *stu-11* also led to an extended

transition zone and synapsis defects (Figure 2.2B, data not shown). Long shifts of *stu-11* mutants did not result in polyploid nuclei, so I did not carry out shorter temperature shifts of this strain.

Only one HIM-8 focus was observed in each meiotic nucleus in *stu-10*, *stu-11*, and *stu-13* hermaphrodites (data not shown), indicating that these functions are dispensable for X chromosome pairing, but may be specifically required for synapsis. To test for autosomal pairing, I stained *stu-11* and *stu-13* mutants for ZIM-2 as a marker for the pairing center of Chromosome V, and found that this autosome, in addition to the X chromosome, pairs robustly in these mutants (Figures 2.2A and 2.3A). Therefore, I conclude that the defects in synapsis observed in these mutant animals did not reflect a defect in homolog pairing. This phenotype is reminiscent of the effects of depleting dynein or dynactin during meiosis.

A closer examination of the pattern of SC loading in these various mutants revealed subtle but distinct differences that may shed light on their specific roles in synapsis. In *stu-11* mutants shifted to the non-permissive temperature, HTP-3 staining was present along chromosomes axes upon meiotic entry, as in wild-type animals (Figure 2.2B). Despite the ability of the chromosomes to pair, however, fully synapsed chromosomes were not observed in early prophase. Instead, the transverse filaments, marked by SYP-1 immunofluorescence, was initially observed as distinct foci along all chromosome axes (Figure 2.2C). In the region of the gonad that normally corresponds to early pachytene, these SYP-1 foci elongated into stretches along chromosome axes, though many chromosomes remained only partially synapsed until late pachytene (Figure 2.2D). These observations suggest that *stu-11* may regulate the processivity of SC polymerization, a process that the lab is working to understand in more detail. The *stu-10(ts)* mutation had been reported to result in a weak Him phenotype even at the permissive temperature (O'Connell et al., 1998), suggestive of a role in meiosis. I was therefore particularly interested in analyzing this mutant. After 24 hours at the restrictive temperature, I observed incomplete synapsis in many meiotic nuclei in *stu-10* mutant animals. In early prophase nuclei, several SYP-1 foci were associated with HTP-3, but failed to extend along entire chromosomes. However, in contrast to the defects in *stu-11* hermaphrodites, I also noticed that some early prophase nuclei showed evidence of improperly assembled chromosome axes, suggesting that *stu-10* may act earlier than *stu-11* by promoting HTP-3 loading and chromosome axis formation (Figure 2.1B). In some nuclei, chromosome axes marked by HTP-3 did not appear as contiguous or as extended as in wild-type animals. The partial axes detected by HTP-3 staining were proficient to load central region components (Figure 2.1C). Thus, it seems likely that the defects in synapsis I observed in *stu-10* mutants reflect an underlying problem with axis assembly Loss of *stu-13* activity, in contrast to both *stu-10* and *stu-11* mutants, resulted in the appearance of large SC polycomplexes in early prophase nuclei, despite apparent normal loading of HTP-3 and homolog pairing (Figure 2.3B and C). These polycomplexes eventually disassembled and

SC central region proteins loaded onto chromosomes in the region of the gonad that normally corresponds to early pachytene (Figure 2.3B). The presence of fully synapsed chromosomes at this stage suggests that *stu-13* may not play an essential role in the processivity of synapsis. Unlike the other mutants that exhibited partial synapsis, chromosomes in *stu-13* mutants were either completely synapsed or unsynapsed, a phenotype that suggests a potential role for *stu-13* in synapsis initiation (Figure 2.3D).

Further investigation into the role of these various mutants will likely shed light on the process of synapsis initiation and polymerization, processes that are not well understood in *C. elegans*. Evidence suggests that synapsis initiation occurs at the PC region of the chromosome (Hayashi et al., 2010; MacQueen et al., 2005), though it is possible that multiple sites of initiation may also contribute to synapsis, particularly in mutant backgrounds. The observation that several SYP-1 foci associate along chromosome axes in *stu-10* and *stu-11* may be indicative of multiple synapsis initiation sites. Future work using *in vivo* imaging may reveal more details about the roles of these genes in timely homologous synapsis.

stu-9 *mutants show defects in chromosome reorganization in early meiosis as well as synapsis*

At the non-permissive temperature, *stu-9* animals displayed multiple meiotic defects. Gonads from *stu-9* mutants were small and contained fewer nuclei than wild-type animals, indicative of a proliferation defect (Fig 2.4A). Meiotic nuclei in early prophase lacked the characteristic chromosome clustering present in transition zone nuclei, and small SUN-1 foci, rather than large patches, were observed at the nuclear envelope (Fig 2.4A and B). Despite the absence of a defined transition zone, homolog pairing of both chromosome V and the X chromosome were robust (Fig 2.4D, data not shown). Synapsis, however, was almost completely abrogated. SYP-1 staining did not appear along chromosome axes, and instead localized diffusely at the nuclear periphery (Fig 2.4C). As described above, most mutants with synapsis defects result in SYP-1 localization to polycomplexes, ordered aggregates of the SC region proteins. The apparent absence of these polycomplexes in *stu-9* mutants indicates that the central region components may not be able to associate properly with each other, since it is known that polycomplex formation requires the presence of all central region components (reviewed in Zickler & Kleckner, 1999).This unique spectrum of phenotypes suggests that identification of the molecular lesion in *stu-9* may illuminate new aspects of meiotic regulation.

stu-15 *mutants show defects in chromosome axis formation*

Like previous *stu* mutants described, *stu-15* animals displayed many polyploid nuclei in the germline when shifted to the non-permissive temperature for 48 hours. Therefore, subsequent analysis was performed after a shorter time shift of 24 hours.

Temperature shifts of *stu-15* hermaphrodites resulted in extensive asynapsis and the presence of SC polycomplexes throughout pachytene (Fig 2.5A and B). Though it has an extended transition zone, nuclei that exhibited a clustered chromosome morphology were often interspersed with those that resembled nuclei from the premeiotic region, in which chromosomes look less condensed and dispersed throughout the nuclear volume. I speculated that defects in synapsis may be caused by an earlier defect in the establishment of proper chromosome axes. Therefore, I tested whether chromosome axes are properly formed in *stu-15* mutants by staining for HTP-3, an axial element component of the SC. I found that HTP-3 loads as distinct foci on chromosomes instead of long tracks, and the foci are associated with central element component SYP-1. The observation that SYP-1 colocalizes with HTP-3 foci suggests that central element loading is not the primary defect, and the inability of chromosomes to synapse in fact stems from a defect in HTP-3 loading and proper chromosome axes formation.

In *stu-15* mutants, the X chromosome pairs robustly but often fails to synapse (Figure 2.5C). While previous data showed that *htp-3* and a normal chromosome axis are required for pairing (Goodyer et al., 2008; Severson et al. 2009), it is possible that sufficient HTP-3 protein is loaded on chromosomes to establish the minimal chromosome structure required for pairing activity in *stu-15* mutants. Moreover, it would be interesting to know whether autosomes pair as robustly as the X chromosome in the absence of normal chromosome axes in *stu-15* mutants. Analysis of homolog pairing in several axial element mutants, including *him-3(me80)* and *htp-1(gk179),* revealed that X chromosomes pair more readily than autosomes (Couteau & Zetka, 2005; Couteau et al., 2004; Martinez-Perez & Villeneuve, 2005; Nabeshima et al., 2004). Additional genetic and cytological analyses will help elucidate the role of *stu-15* in axis formation.

Investigating the role of *spd-3(oj35)* in homolog pairing and synapsis

spd-3(oj35, RNAi) mutants exhibit extensive nonhomologous synapsis

Variable meiotic defects initially observed in *spd-3* animals during the preliminary screen encouraged me to further investigate the role of *spd-3* in homolog pairing and synapsis. But despite multiple experiments, I failed to reproduce the same meiotic phenotype I originally observed. At the non-permissive temperature, *spd-3(oj35)* animals displayed normal pairing and synapsis (data not shown).

In an attempt to push the meiotic phenotype further, I decided to knock down SPD-3 activity by RNAi in *spd-3(oj35)* animals at the non-permissive temperature. The more complete reduction of SPD-3 activity resulted in penetrant meiotic defects in early prophase: large polyploid nuclei with unsynapsed chromosomes and SC polycomplexes (Figure 2.6A and B). These polyploid nuclei seemed to be a direct consequence of the loss of SPD-3 activity. Analysis of *spd-3* null mutants, which contains the *ok1817* deletion allele predicted to

abrogate SPD-3 expression, revealed highly disorganized germlines with large polyploid nuclei (data not shown). The specific defects observed during early prophase seemed to be restricted to that region, however, as nuclei in the mid-pachytene region of the gonad exhibited extensive and often complete synapsis (Figure 2.6C). In these nuclei, the X chromosomes failed to pair, indicating that chromosomes were synapsing nonhomologously in *spd-3(oj35, RNAi)* mutants (Figure 2.6C).

The defects observed in *spd-3(oj35, RNAi)* mutants were dependent on temperature. Synapsis defects were more severe in RNAi-treated mutant animals shifted from 15˚C to 25˚C than those that were shifted to 20˚C. Moreover, the degree of polyploidy greatly decreased. Regardless, *spd-3(oj35, RNAi)* mutants at the lower temperature continued to exhibit non-homologous synapsis (data not shown).

Bacterial diet influences meiotic phenotypes observed in spd-3(oj35) mutants

The effect of feeding *spd-3* dsRNA to *spd-3(oj35)* animals was not specific to the *spd-3* knockdown, however. Subsequent analysis revealed that *spd-3(oj35)* animals fed with RNAi bacteria, regardless of the dsRNA produced, resulted in extensive nonhomologous synapsis (Figure 2.7A). *spd-3(oj35)* animals were fed with RNAi bacteria producing dsRNA against *rfp-1* and *K12H4.2*, two potential yeast two-hybrid interactors of SPD-3 that were later confirmed as false-positives (see Materials and Methods). Additionally, *spd-3(oj35)* animals were fed with RNAi bacteria producing dsRNA against *wapl-1* and *fkb-6,* two genes expressed in the germline but whose knockdown in the wild-type background yielded no meiotic phenotype (Abby Dernburg, personal communication). In all of these cases, extensive nonhomologous synapsis was observed in the *spd-3(oj35)* background but not in wild-type (Figure 2.7A, data not shown).

To test whether RNAi induced nonhomologous synapsis, I fed animals bacteria containing the empty RNAi vector L4440, which does not produce dsRNA. Surprisingly, I found that feeding *spd-3(oj35)* animals HT115 bacteria on RNAi plates was sufficient to induce nonhomologous synapsis (Figure 2.6B). I further tested whether the addition of antibiotics or IPTG in the RNAi plates caused the same effect in the *spd-3(oj35)* background. I transferred *spd-3(oj35)* animals onto an RNAi plate spotted with OP50 bacteria. Because I did not observe a meiotic defect with animals fed with OP50, I concluded that feeding *spd-3(oj35)* animals HT115 bacteria was sufficient to cause nonhomologous synapsis (Figure 2.6C).

SPD-3 localizes outside of germline nuclei

Due to the specific meiotic defects observed in *spd-3* loss-of-function mutants and the protein's predicted transmembrane domains, I speculated that SPD-3 would localize with SUN-1/ZYG-12 patches at the nuclear envelope. Previous studies on the role of *spd-3* in development showed that SPD-3 protein localizes to the mitochondria in the early embryo (Dinkelmann et al., 2007). Without a proper SPD-3 antibody, I used the allele *ojIs33* which expresses

spd-3::gfp under the *pie-1* promoter from a high-copy array insertion to observe its localization in the germline. I first verified that SPD-3::GFP is functional by crossing the allele into *spd-3(ok1817)*. The transgene complements defects in *ok1817* animals, rescuing the sterile and embryonic lethal phenotypes associated with the loss of SPD-3 activity. SPD-3::GFP did not colocalize with patches at the nuclear envelope. Instead, the protein appeared to localize everywhere outside of the nucleus, in the cytoplasm and the rachis of the gonad. (Figure 2.6A).

To look at whether SPD-3 localizes to the mitochondria, I used a combination of antibodies against two known mitochondrial proteins, cytochrome c and ATP synthase, as well as an antibody against GFP (Pourkarimi, Greiss, & Gartner, 2011). Although the mitochondria and SPD-3 seemed to display a similar localization pattern in the germline, their signals often converged on one another but rarely overlapped (Fig 2.6B). It is possible that SPD-3 has a different subcellular localization in the germline than in embryos.

I next tested whether SPD-3 may be associating with the endoplasmic reticulum (ER) in the germline. I performed similar immunofluorescence experiments, this time using an antibody which recognizes the specific sequence HDEL, an ER-retention signal (Basham & Rose, 2001). However, I discovered that SPD-3 did not localize to the ER (Fig 2.6B). The exact subcellular localization of SPD-3 remains to be determined.

Additional questions and future directions

My observations that bacterial diet can influence meiotic phenotypes and induce nonhomologous synapsis in the *spd-3(oj35)* background is unprecedented and several major questions remain. In particular, the specific activity of SPD-3 and its localization remains to be determined. By identifying SPD-3 interactors, we can begin to speculate where and how it functions during meiosis. Meanwhile, I offer three different contexts by which SPD-3 may possibly affect meiotic prophase.

The observation that a cytoplasmic protein can have significant effects on meiotic events within the nucleus is not unprecedented. Ronceret et al. (2009) showed that PHS1 functions by controlling transport of RAD50, a meiotic recombination protein, into the nucleus. The PHS1 protein forms discrete granules throughout the cytoplasm (Ronceret et al., 2009). In its absence, chromosomes undergo extensive nonhomologous synapsis. It is therefore possible that SPD-3 may indirectly affect meiosis by sequestering essential meiotic proteins or affecting their functions in early prophase.

An alternative explanation can be derived from recent studies of the role of Mps3 in budding yeast. Mps3, a SUN protein and SPB component, was shown to function in lipid homeostasis (Friederichs et al., 2001). Cells lacking *MPS3* contain abnormal amounts of certain types of lipids. Furthermore, altering the lipid composition of Mps3 mutants, by culturing strains in various media, suppressed their growth defects. Therefore, it is possible that *spd-3* mutants fed with various bacteria may alter the lipid composition of the nuclear envelope, thereby altering

meiotic chromosome dynamics. Studies from another lab which showed that bacterial diet can influence fat storage in *C. elegans* further supports this idea (Brooks et al., 2009) Biochemical lipid analysis of *spd-3* mutants will begin to validate this hypothesis.

Finally, the discovery that SPD-3 closely associates with the mitochondria in the germline may suggest that SPD-3 functions in metabolism and regulating the energy required for proper chromosome dynamics. Analyzing meiotic chromosome dynamics by a GFP-tagged HIM-8 (Wynne et al., unpublished) or the LacI/LacO system (described below) can begin to address this hypothesis.

Implementing the LacI/LacO system to visualize specific genomic loci in *C. elegans*

Although we can learn a significant amount of information about meiotic prophase events by using cytological tools such as immunofluorescence and in situ hybridization, the information we can gather with fixed images remains limited. In *C. elegans,* live imaging of early prophase nuclei was achieved by expressing GFP-tagged nuclear envelope patch components SUN-1 and ZYG-12 (Baudrimont et al., 2010; Wynne et al, unpublished.). These studies revealed that chromosome ends at nuclear envelope patches are highly dynamic but could not distinguish between chromosomes nor reveal information about the dynamics at non-PC ends. A GFP-tagged HIM-8 enabled the specific analysis of X chromosome dynamics, but a tagged autosomal ZnF protein has yet to be made (Wynne et al., unpublished).

Cis- and *trans*-acting components of the *lac* operon from *E. coli* were first exploited to enable targeting of proteins to specific chromosomal loci in yeast (Robinett et al., 1996; Straight et al., 1996). The Lac repressor, encoded by the LacI gene, specifically binds to a DNA sequence called the Lac operator or LacO. Tagging the repressor with GFP allowed visualization of specific loci containing integrated LacO arrays (Belmont & Straight, 1998). Using this system in *S. pombe* to study chromosome dynamics *in vivo* revealed that pairing is a highly dynamic process; homologous loci associate and dissociate multiple times in the course of meiosis (Ding et al., 2004). I implemented the LacI/LacO system in *C. elegans* as a way to broaden our toolkit for live imaging of meiotic chromosomes.

To do this, I utilized a novel transposon-based technique, MosSCI, to generate targeted insertions at various specific locations in the genome (Frøkjaer-Jensen et al., 2008). MosSCI is based on the repair of an induced double-strand break, by mobilization of a Mos1 transposon, from an extrachromosomal donor template. The location of the Mos1 transposon defines the insertion site. To mark several different chromosomal loci, I chose four separate *Mos1* alleles at the PC and non-PC ends of the X chromosome and chromosome III based on their genomic location and the additional criteria that the insertion: 1) was not within the coding region of a gene 2) was not located immediately upstream or downstream of a nearby gene (Table 2). I engineered a specific targeting vector for each allele

which contains 256 copies of the LacO sequence and *unc-119+* rescuing marker, flanked by homologous sequences surrounding the *Mos1* element (Figure 2.8A). The LacO strains generated by MosSCI were initially verified by PCR using a forward primer that recognized a sequence upstream of the *Mos1* site and a reverse primer that recognized a sequence in the *unc-119+* gene (data not shown). Because PCR merely confirmed that *unc-119+* was inserted at the correct genomic position, I needed further verification that the LacO array was present. I confirmed this by performing FISH against the array itself (data not shown).

The biggest challenge in implementing this system was expressing GFP-LacI in the germline. In *C. elegans,* germline expression is notoriously difficult to attain. High-copy arrays which are commonly used for somatic expression are silenced in the germline due to a poorly understood epigenetic mechanism that likely senses the high copy-number or repetitive nature of extrachromosomal arrays (Dernburg et al., 2000; Mello & Fire, 1995). This problem was partially circumvented by the development of biolistic transformation which integrates transgenes into the genome in low-copy number and in a non-targeted and mostly random manner (Wilm et al., 1999). However, even those low-copy insertions (and sometimes single-copy insertions generated by MosSCI) are subject to poorly understood epigenetic silencing (Frøkjaer-Jensen et al., 2008). Furthermore, germline expression is limited by the lack of information on regulatory elements required to recapitulate endogenous germline expression, although systematic studies have been done which showed that 3' UTRs often specify expression patterns (Merritt et al., 2008). Due to these challenges, I utilized a combination of recombineering and biolistic transformation in an attempt to express GFP-LacI in the germline.

Recombineering is a tool that allows insertion of tags at the target gene locus within large genomic clones by homologous recombination, and has been established in *C. elegans* as an alternative to conventional reporter gene approaches (Dolphin & Hope, 2006; Sarov et al., 2006; Tursun et al., 2009). The key advantage of recombineering is the ability to express genes within the context of endogenous *cis*-regulatory elements. I aimed to express GFP-LacI within the context of *zyg-12* regulatory elements. *zyg-12* is expressed in the mitotic and meiotic germline and in the early embryo (Malone et al., 2003). Using the toolkit and pipeline developed in the Hobert lab, I replaced the *zyg-12* coding region with that of GFP-LacI, and introduced the recombineered fosmid into *C. elegans* by biolistic transformation. I successfully generated one line which expressed GFP-LacI in the germline and embryo and named the allele *ieIs29.*

I tested whether GFP-LacI can bind to the LacO insertion array at the X chromosome PC by crossing *ieIs29* into *ieSi2*, the insertion allele of LacO at the X chromosome PC. By immunofluorescence I verified that GFP-LacI binds to chromosomes and forms foci which colocalize with HIM-8 (Figure 2.8B). Initial observations showed bright foci as well as diffused GFP signal in the nucleus which was readily detected by eye (Figure 2.8C). Several weeks later, however,

the signal had become very dim and many animals no longer had detectable GFP signal in the germline (Figure 2.8C). Outcrossing or selecting animals with the strongest GFP expression did not solve the problem of silencing and eventually the line no longer expressed GFP-LacI. It is possible that this particular line had an insertion with a high-copy number that induced silencing. Generating additional lines may yield a stable line expressing GFP-LacI. Alternatively, transgenic lines can also be made by MosSCI which would limit the insertion size and thus risk exclusion of essential *cis*-regulatory elements.

Using a spinning-disk confocal microscope to image meiotic chromosomes in *ieIs29; ieSi2*, I discovered that PC ends of paired X chromosomes can be resolved into two distinct GFP foci, a clear advantage to imaging with this system as opposed to tagged ZnF proteins like HIM-8 which presents paired PCs as a globular focus, due to the large region (1Mb) comprising the HIM-8 binding motif (Phillips et al., 2009). In contrast, the LacO array insertion spans a much smaller 10-kb region. A short movie of captured evidence that may support our current model for homolog pairing and synapsis: “splitting” events between paired homologous loci (data not shown). During these events, one of two GFP foci from a set of paired X chromosomes rapidly moved in one direction while the other, which had remained motionless, immediately followed after. These events were also captured by imaging with GFP-tagged HIM-8 where stretches of the HIM-8 focus were observed after pairing (Wynne et al., unpublished). We speculate that this behavior reflects dynein-driven opposing forces that act on paired chromosomes to assess homology and license synapsis initiation. Additional efforts must be made to characterize these events during normal meiosis, dynein loss-of-function mutants, and other mutants which affect chromosome motion, including *stu* mutants described previously. Furthermore, it would be interesting to combine this system with a tagged central element component to observe synapsis initiation with respect to these events.

Preliminary studies using tools I generated by implementing the LacI/LacO system in *C. elegans* reveal their potential applications in live imaging of meiotic chromosomes. This system would enable the study of dynamics of specific chromosomal loci in a variety of mutant backgrounds. Additionally, this system may be able to overcome the limited expression and localization pattern of the currently available constructs, which allows imaging only up to early pachytene. The LacI/LacO system could, in principle, be used to visualize segregation of specific chromosomes during meiotic divisions or as an artificial tethering system to localize chromosomes to the nuclear envelope or to another chromosome.

Materials and Methods

Worm strains and culture conditions

All worms were cultured according to standard conditions at 20°C or 15°C unless otherwise noted {Brenner:1974wn}. Strains used in this study are listed on Table 1, as well as *spd-3(ok1817)* and WH344. N2 Bristol strain was used for the wild-type control. The catalog of mutants used for the candidate screen were made available by the *Caenorhabditis elegans* Genetics Center.

RNAi by feeding

RNAi targeting of *spd-3, wapl-1, fkb-6, K12H4.2* and *rfp-1* was performed with clones from the Ahringer library and the L4440 empty RNAi vector was used as a negative control {Fraser:2000hl}. Bacterial cultures were grown in LB +antibiotics overnight and concentrated 20-fold. 50μl was spread on 60mm NGM plates with 1mM IPTG and antibiotics. Production of double-stranded RNA was induced overnight at 37˚C overnight. Wild-type or *spd-3(oj35)* L4 animals grown at 15˚C were transferred to a small pool of M9 buffer on a freshly prepared RNAi plate, allowed to crawl for 1-2 hours at room temperature, transferred to a new RNAi plate at 20˚C or 25˚C, and dissected 24 or 48 hours later.

Bacterial cultures of OP50 and HT115 were grown at 37˚C overnight with shaking. 50μl of a saturated culture was spread on 60mm NGM plates and allowed to dry overnight. Wild-type or *spd-3(oj35)* L4 animals grown on OP50-seeded plates at 15˚C were transferred to a new plate seeded with bacteria, allowed to crawl around for 1-2 hours at room temperature, then transferred to a new plate with the same type of bacteria to minimize OP50 contamination via transfer from the original plate. Animals were grown at 15˚C or 25˚C and dissected 48 hours later.

Antibodies and cytological assays

Immunofluorescence was performed as previously described {Phillips: 2009ct}. Young adult hermpahrodites were dissected in egg buffer containing sodium azide and .1% Tween-20, fixed for 2-3 minutes in egg buffer+1% formaldehyde between a Histobond slide and coverslip, and frozen on dry ice. The coverslip was removed and slides were transferred to -20˚C methanol for 1 minute. Slides were transferred to PBST(containing .1% Tween-20), washed in 2 further changes of PBST, blocked with Roche blocking agent for 20 minutes, and stained with primary antibodies for 2 hours at room temperature or overnight at 4˚C. Following 3 consecutive washes with PBST, slides were stained with secondary antibodies labeled with Alexa 488, Cy3 or Cy5 for 1-2 hours at room temperature. Slides were washed with 3 consecutive times in PBST, with the second wash containing .5ug/ml DAPI to stain chromosomes, and mounted in glycerol-based mounting medium containing n-propyl gallate.

To stain mitochondria, a 1:200 dilution of anti-ATP synthase (MS507) and anti-cytochrome c (MS A06) was used (MitoSciences). The ER was stained with anti-HDEL at a 1:250 dilution (Santa Cruz Biotechnologies).

Fluorescence in situ hybridization (FISH) procedures have also been previously described in detail {Phillips:2009ct}. A LacO FISH probe was created using an oligo which includes the 36-bp LacO sequence (ccacatgtggaattgtgagcggataacaatttgtgg).

Images were acquired using a DeltaVision RT system (Applied Precision) equipped with a 100x N.A. 1.40 oil-immersion objective (Olympus), resulting in an effective XY pixel spacing of 0.067 or 0.045 μm. 3D image stacks were collected at .2μm Z-spacing and processed by constrained, iterative deconvolution. Image scaling and analysis were performed using functions in the softWorx software package. Projections were calculated by a maximum intensity algorithm. Composite images were assembled and false colorizing performed with Adobe Photoshop.

Yeast two-hybrid screen

Yeast 2-hybrid screening was performed using the ProQuest Two-Hybrid System (Invitrogen). A poly-T-primed cDNA library was constructed from young adult hermaphrodites and cloned into pDEST22. The coding sequence of SPD-3 (aa 74-479) was amplified by RT-PCR, sequence-verified, and cloned into pDEST32. Of the candidate interactors identified from the screen, pairwise assays between *spd-3* and *rfp-1* or *K12H4.2* was performed. Full length cDNA sequences of *rfp-1* and *K12H4.2* was amplified by RT-PCR, sequence-verified and cloned into pDEST22.

Generating GFP-LacI and LacO array insertion strains

A GFP cassette containing introns from the toolkit generated by the Hobert Lab was cloned upstream of the LacI gene in pAFS135. The resulting GFP-LacI sequence was amplified and recombineered into fosmid WRM062a06 to replace the *zyg-12* gene as described (Tursun et al., 2009) to generate pREG33. The recombineered fosmid was transformed in *unc-119(ed3)* by biolistic transformation (Merritt & Seydoux, 2010).

The donor template to generate LacO array strains were created by a series of cloning experiments. The multiple cloning site fragment from the empty RNAi vector L4440 was PCR amplified with primers containing appropriate *att* overhangs and cloned into pDONR22 using Gateway ™ technology (Invitrogen). A 10-kb fragment containing 256 copies of the LacO sequence from pAFS52 was cloned into the the HindIII and KpnI sites, resulting in pREG27. *C. briggsae unc-119+* gene was PCR amplified from pRL8 with primers containing NcoI site overhangs and cloned into pREG27. The resulting vector (pREG38) was used in subsequent reactions using the Multi-Site Gateway™ technology to generate specific donor templates. Approximately ~1.5-kb of sequence immediately to the left and right of each *Mos1* allele was amplified and cloned into pDONR P4-P1R

and pDONR P2R-P3, respectively. The resulting vectors were used in conjunction with pREG38 to create MosSCI donor plasmids.

Various Mos1 alleles (Table 1) were received from the Segalat lab and crossed into *unc-119(ed3)*. Genotyping by PCR verified that these strains were homozygous for the *Mos1* insertion and injected with the appropriate donor template, pJL43.1, pGH8, pCFJ90 and pCFJ104, as described (Frokjaer-Jensen et al., 2010). Non-Unc, mCherry-minus progeny were identified after several generations. Successful insertions were verified by PCR.

References

Basham, S. E., & Rose, L. S. (2001). The Caenorhabditis elegans polarity gene ooc-5 encodes a Torsin-related protein of the AAA ATPase superfamily *Development (Cambridge, England)*, *128*(22), 4645–4656.

Baudrimont, A., Penkner, A., Woglar, A., Machacek, T., Wegrostek, C., Gloggnitzer, J., Fridkin, A., et al. (2010). Leptotene/zygotene chromosome movement via the SUN/KASH protein bridge in Caenorhabditis elegans *PLoS genetics*, *6*(11), e1001219. doi:10.1371/journal.pgen.1001219

Belmont, A. S., & Straight, A. F. (1998). In vivo visualization of chromosomes using lac operator-repressor binding *Trends in cell biology*, *8*(3), 121–124.

Brooks, K. K., Liang, B., Watts, J. L. (2009). The Influence of Bacteria on Fat Storage in *C. elegans. PLoS ONE* 4(10): e7545. doi: 10.1371/journal.pone. 0007545

Couteau, F., & Zetka, M. (2005). HTP-1 coordinates synaptonemal complex assembly with homolog alignment during meiosis in C. elegans *Genes & development*, *19*(22), 2744–2756. doi:10.1101/gad.1348205

Couteau, F., Nabeshima, K., Villeneuve, A., & Zetka, M. (2004). A component of C. elegans meiotic chromosome axes at the interface of homolog alignment, synapsis, nuclear reorganization, and recombination *Current biology : CB*, *14*(7), 585–592. doi:10.1016/j.cub.2004.03.033

Dernburg, A. F., Zalevsky, J., Colaiácovo, M. P., & Villeneuve, A. M. (2000). Transgene-mediated cosuppression in the C. elegans germ line *Genes & development*, *14*(13), 1578–1583.

Ding, D.-Q., Yamamoto, A., Haraguchi, T., & Hiraoka, Y. (2004). Dynamics of homologous chromosome pairing during meiotic prophase in fission yeast *Developmental cell*, *6*(3), 329–341.

Dinkelmann, M. V., Zhang, H., Skop, A. R., & White, John G. (2007). SPD-3 is required for spindle alignment in Caenorhabditis elegans embryos and localizes to mitochondria *Genetics*, *177*(3), 1609–1620. doi:10.1534/genetics.107.078386

Dolphin, C. T., & Hope, I. A. (2006). Caenorhabditis elegans reporter fusion genes generated by seamless modification of large genomic DNA clones *Nucleic acids research*, *34*(9), e72. doi:10.1093/nar/gkl352

Friederichs J.M., Ghosh, S., Smoyer C.J., McCroskey S., Miller B.D., et al. (2011) The SUN Protein Mps3 is Required for Spindle Pole Body Insertion into the Nuclear Membrane and Nuclear Envelope Homeostasis. *PLoS Genetics* 7 (11):e1002365. doi:10.1371/journal.pgen.1002365

Frøkjaer-Jensen, C., Davis, M. W., Hopkins, C. E., Newman, B. J., Thummel, J. M., Olesen, S.-P., Grunnet, M., et al. (2008). Single-copy insertion of transgenes in Caenorhabditis elegans *Nature genetics*, *40*(11), 1375–1383. doi:10.1038/ng.248

Golubovskaya, I.N., Harper, L.C., Pawlowski, W.P., Schichnes, D., and Cande, W.Z. (2002) The *pam1* gene is required for meiotic bouquet formation and efficient homologous synapsis in maize. *Genetics 162,* 1979-1993.

Goodyer, W., Kaitna, S., Couteau, F., Ward, J. D., Boulton, S. J., & Zetka, M. (2008). HTP-3 links DSB formation with homolog pairing and crossing over during C. elegans meiosis *Developmental cell*, *14*(2), 263–274. doi:10.1016/j.devcel.2007.11.016
Gönczy, P., Pichler, S., Kirkham, M., & Hyman, A. A. (1999). Cytoplasmic dynein is required for distinct aspects of MTOC positioning, including centrosome separation, in the one cell stage Caenorhabditis elegans embryo *The Journal of cell biology*, *147*(1), 135–150.
Hayashi, M., Mlynarczyk-Evans, S., & Villeneuve, A. M. (2010). The synaptonemal complex shapes the crossover landscape through cooperative assembly, crossover promotion and crossover inhibition during Caenorhabditis elegans meiosis *Genetics*, *186*(1), 45–58. doi:10.1534/genetics.110.115501
MacQueen, A. J., Phillips, C. M., Bhalla, N., Weiser, P., Villeneuve, A. M., & Dernburg, A. F. (2005). Chromosome sites play dual roles to establish homologous synapsis during meiosis in C. elegans *Cell*, *123*(6), 1037–1050. doi:10.1016/j.cell.2005.09.034
Malone, C. J., Misner, L., Le Bot, N., Tsai, M.-C., Campbell, J. M., Ahringer, J., & White, J. G. (2003). The C. elegans hook protein, ZYG-12, mediates the essential attachment between the centrosome and nucleus *Cell*, *115*(7), 825–836.
Martinez-Perez, E., & Villeneuve, A. M. (2005). HTP-1-dependent constraints coordinate homolog pairing and synapsis and promote chiasma formation during C. elegans meiosis *Genes & development*, *19*(22), 2727–2743. doi:10.1101/gad.1338505
Mello, C., & Fire, A. (1995). DNA transformation *Methods in cell biology*, *48*, 451–482.
Merritt, C., & Seydoux, G. (2010). Transgenic solutions for the germline *WormBook : the online review of C. elegans biology*, 1–21. doi:10.1895/wormbook.1.148.1
Merritt, C., Rasoloson, D., Ko, D., & Seydoux, G. (2008). 3' UTRs are the primary regulators of gene expression in the C. elegans germline *Current biology : CB*, *18*(19), 1476–1482. doi:10.1016/j.cub.2008.08.013
Nabeshima, K., Villeneuve, A. M., & Hillers, K. J. (2004). Chromosome-wide regulation of meiotic crossover formation in Caenorhabditis elegans requires properly assembled chromosome axes *Genetics*, *168*(3), 1275–1292. doi:10.1534/genetics.104.030700
O'Connell, K. F., Leys, C. M., & White, J G. (1998). A genetic screen for temperature-sensitive cell-division mutants of Caenorhabditis elegans *Genetics*, *149*(3), 1303–1321.
Penkner, A., Tang, L., Novatchkova, M., Ladurner, M., Fridkin, A., Gruenbaum, Y., Schweizer, D., et al. (2007). The nuclear envelope protein Matefin/SUN-1 is required for homologous pairing in C. elegans meiosis *Developmental cell*, *12*(6), 873–885. doi:10.1016/j.devcel.2007.05.004

Pourkarimi, E., Greiss, S., & Gartner, A. (2011). Evidence that CED-9/Bcl2 and CED-4/Apaf-1 localization is not consistent with the current model for C. elegans apoptosis induction *Cell death and differentiation*. doi:10.1038/cdd.2011.104
Robinett, C. C., Straight, A., Li, G., Willhelm, C., Sudlow, G., Murray, A., & Belmont, A. S. (1996). In vivo localization of DNA sequences and visualization of large-scale chromatin organization using lac operator/repressor recognition *The Journal of cell biology*, *135*(6 Pt 2), 1685–1700.
Ronceret, A., Marie-Pascale, D., Bolubovskaya, I. N., Pawlowski, W. P. (2009) PHS1 regulates meiotic recombination and homologous chromosome pairing by controlling the tansport of RAD50 and MRE11 to the nucleus. *PNAS* 106(47), 20121-20126.
Sarov, M., Schneider, S., Pozniakovski, A., Roguev, A., Ernst, S., Zhang, Y., Hyman, A. A., et al. (2006). A recombineering pipeline for functional genomics applied to Caenorhabditis elegans *Nature methods*, *3*(10), 839–844. doi:10.1038/nmeth933
Sato, A., Isaac, B., Phillips, C. M., Rillo, R., Carlton, P. M., Wynne, D. J., Kasad, R. A., et al. (2009). Cytoskeletal forces span the nuclear envelope to coordinate meiotic chromosome pairing and synapsis *Cell*, *139*(5), 907–919. doi:10.1016/j.cell.2009.10.039
Schmidt, D. J., Rose, D. J., Saxton, W. M., & Strome, S. (2005). Functional analysis of cytoplasmic dynein heavy chain in Caenorhabditis elegans with fast-acting temperature-sensitive mutations *Molecular biology of the cell*, *16*(3), 1200–1212. doi:10.1091/mbc.E04-06-0523
Severson, A. F., Ling, L., van Zuylen, V., & Meyer, B. J. (2009). The axial element protein HTP-3 promotes cohesin loading and meiotic axis assembly in C. elegans to implement the meiotic program of chromosome segregation *Genes & development*, *23*(15), 1763–1778. doi:10.1101/gad.1808809
Sheehan, M.J., Pawlowski, W.P., 2009. Live imaging of rapid chromosome movements in meiotic prophase I in maize. *PNAS* 106: 20989-20994.
Straight, A. F., Belmont, A. S., Robinett, C. C., & Murray, A. W. (1996). GFP tagging of budding yeast chromosomes reveals that protein-protein interactions can mediate sister chromatid cohesion *Current biology : CB*, *6*(12), 1599–1608.
Tursun, B., Cochella, L., Carrera, I., & Hobert, O. (2009). A toolkit and robust pipeline for the generation of fosmid-based reporter genes in C. elegans *PloS one*, *4*(3), e4625. doi:10.1371/journal.pone.0004625
Wilm, T., Demel, P., Koop, H. U., Schnabel, H., & Schnabel, R. (1999). Ballistic transformation of Caenorhabditis elegans *Gene*, *229*(1-2), 31–35.
Zickler, D., & Kleckner, N. (1999). Meiotic chromosomes: integrating structure and function *Annual review of genetics*, *33*, 603–754. doi:10.1146/annurev.genet.33.1.603

genotype	pairing	synapsis	NE patches
stu-8(oj1)	✓	✓	✓
spd-1(oj1)	✓	✓	✓
stu-9(oj13)	✓	asynapsis	extended
stu-10(oj14)	✓	asynapsis	extended
stu-11(oj18)	✓	asynapsis	extended
stu-12(oj21)	✓	✓	✓
slo-1(oj23)	✓	✓	✓
stu-13(oj24)	✓	asynapsis	extended
stu-14(oj26)	✓	✓	✓
stu-15(oj28)	✓	asynapsis + polycomplexes	extended
spd-2(oj29)	✓	✓	✓
stu-16(oj30)	✓	✓	✓
stu-17(oj31)	✓	✓	✓
stu-18(oj32)	✓	✓	✓
stu-19(oj33)	✓	✓	✓
spd-3(oj35)	*delayed	*delayed	*extended

Table 1. Preliminary results from a candidate screen for novel meiotic regulators of chromosome dynamics. Mutant strains were shifted to 25°C at the L4 stage for 48 hours. Pairing, synapsis and the presence of nuclear envelope aggregates in the transition zone were assayed by immunofluorescence using antibodies against HIM-8, SYP-1 and SUN-1, respectively. *Meiotic defects observed in *spd-3(oj35)* animals were not reproducible in subsequent experiments.

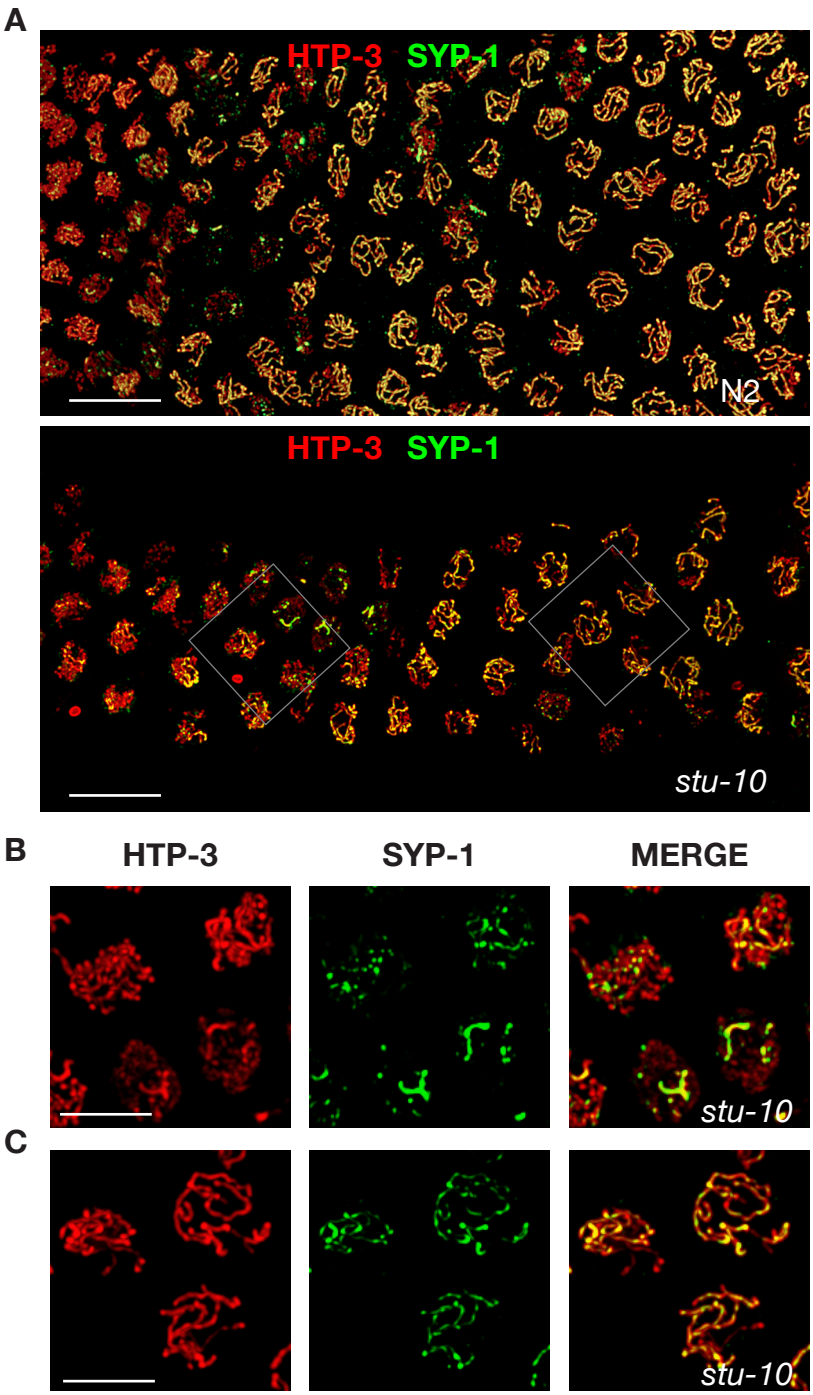

Figure 2.1 ***stu-10*** **animals display defects in synapsis and chromosome axis formation** (A) Composite projection images of gonads from a wild-type N2 and *stu-10(oj14)* animal that was shifted to 25˚C at the L4 stage for 24 hours and stained with anti-HTP-3 (axial element protein, red) and anti-SYP-1 (central element protein, green). Nuclei from early prophase up to early pachytene are shown. Meiotic progression is from left to right. Scale bar, 15µM. (B) Higher-

magnification of nuclei from early prophase is shown. SYP-1 loads on chromosome axes in a punctate manner and some nuclei fail to properly load HTP-3 in *stu-10(oj14)* mutants. Scale bar, 5μM. (C) Higher-magnification of nuclei from early pachytene. Extensive but incomplete synapsis is achieved in the *stu-10(oj14)* mutant. Scale bar, 5μ.

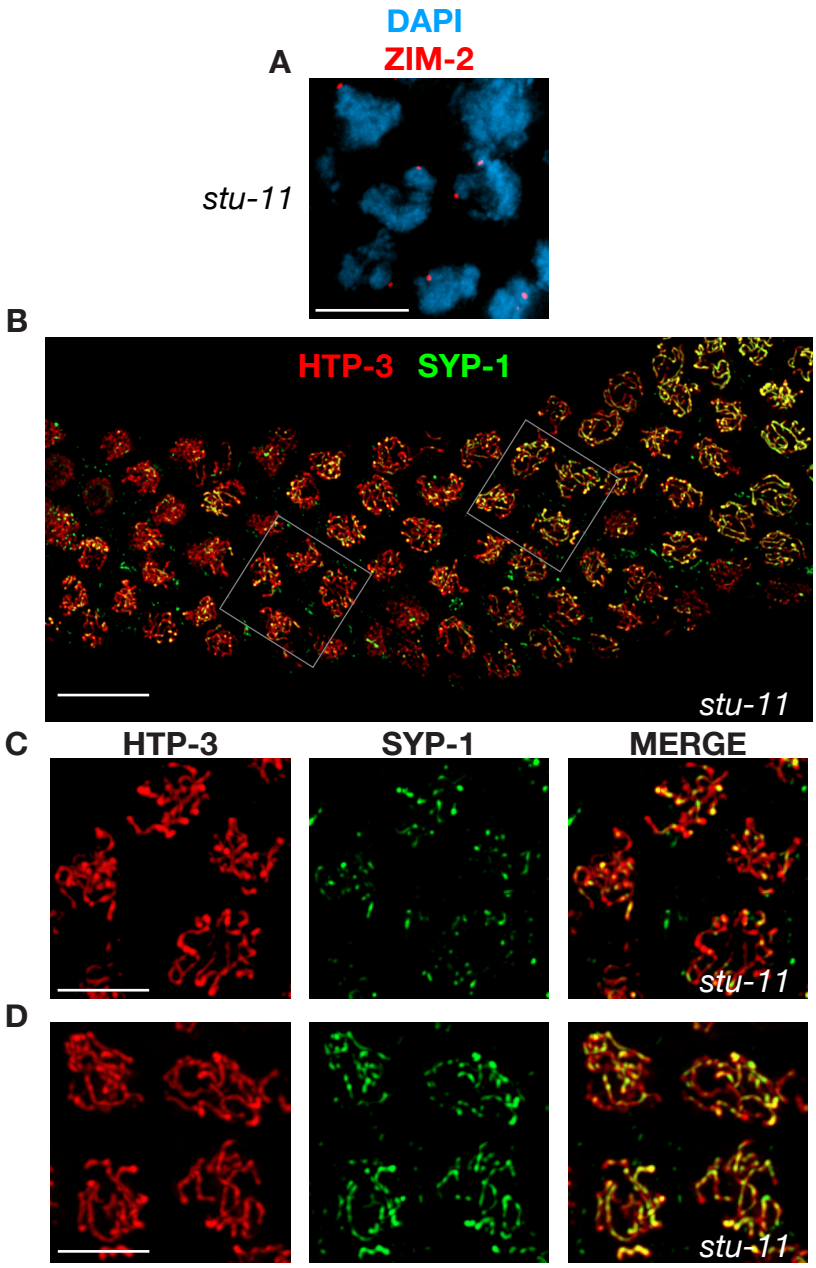

Figure 2.2 *stu-11* animals display defects in synapsis despite robust homolog pairing (A) Field of early prophase nuclei from a *stu-11(oj18)* animal that was shifted to 25˚C at the L4 stage for 24 hours and stained with DAPI (chromosomes, blue) and anti-ZIM-2 (chromosome V PC ZnF protein, red). Pairing is robust in *stu-11(oj18)* animals. Scale bar, 5µM. (B) Composite projection images of a gonad from a *stu-11(oj18)* animal stained with anti-HTP-3 (red) and anti-SYP-1 (green). Nuclei from early prophase and a portion of

pachytene are shown. Scale bar, 15µM. (B) Higher-magnification of nuclei from early prophase is shown. SYP-1 loads on chromosome axes in a punctate manner in *stu-11(oj18)* mutants. Scale bar, 5µM. (C) Higher-magnification of nuclei from early pachytene. Extensive but incomplete synapsis achieved in *stu-11(oj18)* mutants. Scale bar, 5µM.

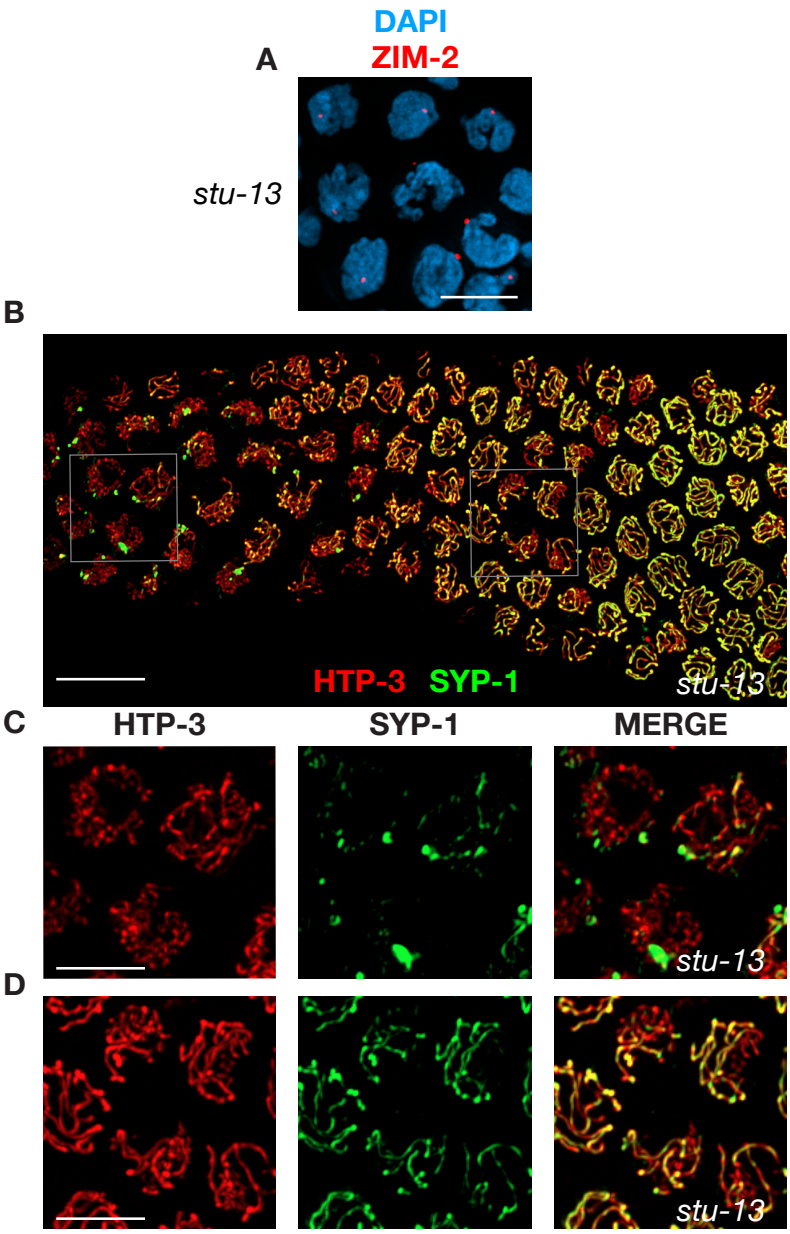

Figure 2.3 *stu-13* animals exhibit delays in synapsis initiation (A) Field of early prophase nuclei from a *stu-13(oj24)* animal that was shifted to 25˚C at the L4 stage for 48 hours and stained with DAPI and anti-ZIM-2. Pairing is robust in *stu-13(oj24)* mutants. Scale bar, 5μM. (B) Composite projection images of a gonad from a *stu-13(oj24)* animal stained with anti-HTP-3 and anti-SYP-1. Nuclei from early prophase and part of pachytene are shown. Meiotic progression is from left to right. Scale bar, 15μM. (C) Higher-magnification of nuclei from early prophase is shown. HTP-3 loads on chromosomes, but SC polycomplexes are present and chromosomes remain largely unsynapsed. Scale bar, 5μM. (D) Higher-magnification of nuclei from early pachytene. SC polycomplexes have dematerialized and extensive but incomplete synapsis is achieved in *stu-13(oj24)* mutants. Scale bar, 5μM.

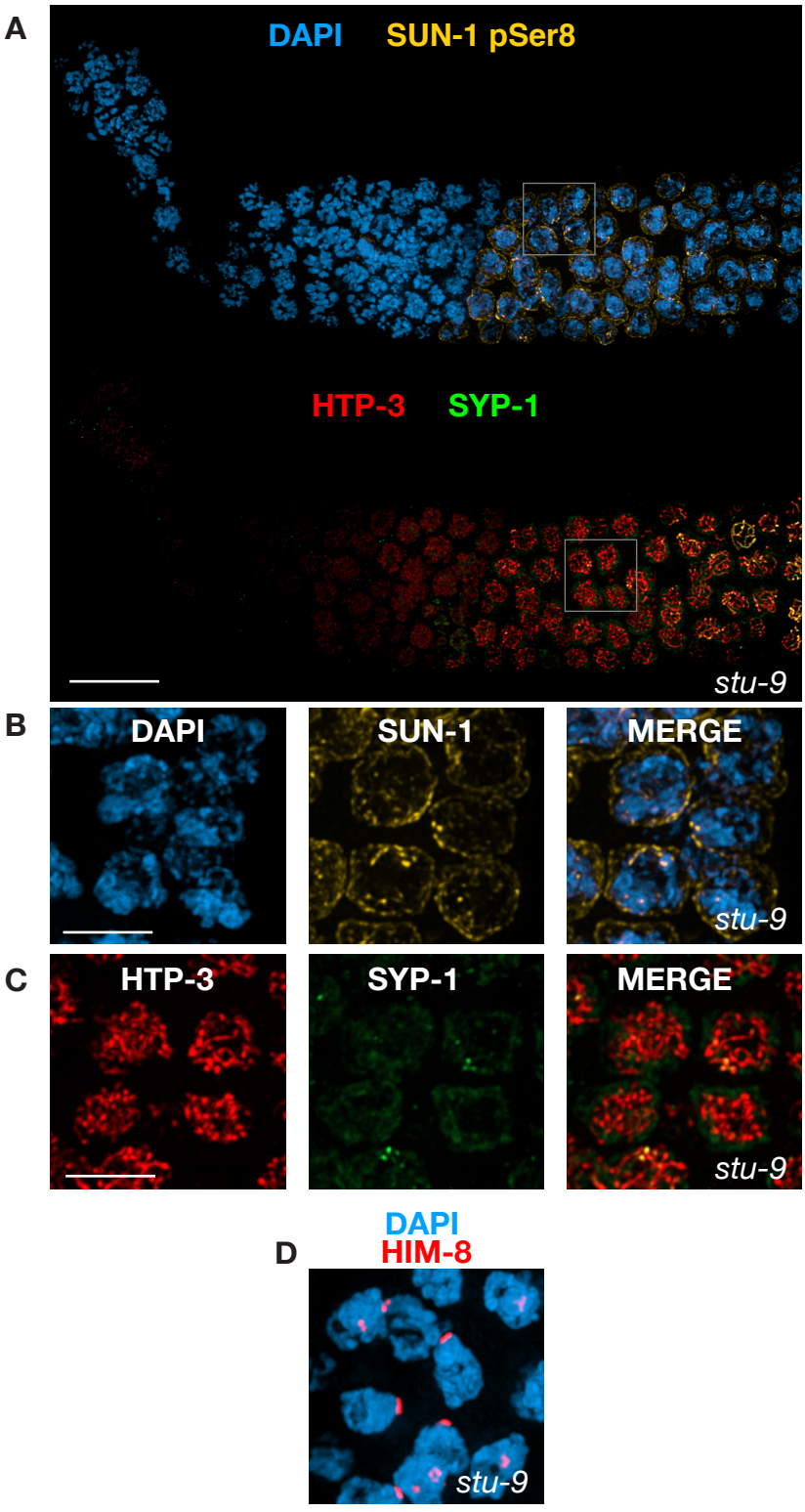

Figure 2.4 *stu-9* animal exhibit defects in chromosome reorganization and synapsis (A) Composite projection images of a gonad from a *stu-9(oj13)* animal

that was shifted to 25˚C at the L4 stage for 48 hours and stained with DAPI, anti-SUN-1 Ser8-Pi (yellow), anti-HTP-3 (red), and anti-SYP-1 (green). Meiotic progression is from left to right. Nuclei from distal tip to region corresponding to late pachytene are shown. *stu-9* animals have a small gonad and very few meiotic nuclei. Scale bar, 15μM. (B) Higher-magnification of nuclei stained with DAPI and anti-SUN-1 Ser8-Pi is shown. Chromosomes remain dispersed evenly throughout the nuclear volume and NE patches are absent. Scale bar, 5μM. (C) Higher-magnification of nuclei stained with anti-HTP-3 and anti-SYP-1 is shown. Chromosomes completely fail to synapse. Diffuse SYP-1 localization at the nuclear periphery is present in *stu-9(oj13)* mutants. Scale bar, 5μM. (D) Field of meiotic nuclei from *stu-9(oj13)* mutants stained with DAPI and anti-HIM-8 (X chromosome PC ZnF protein, red). Pairing of X chromosomes is robust in *stu-9 (oj13)* mutants. Scale bar, 5μM.

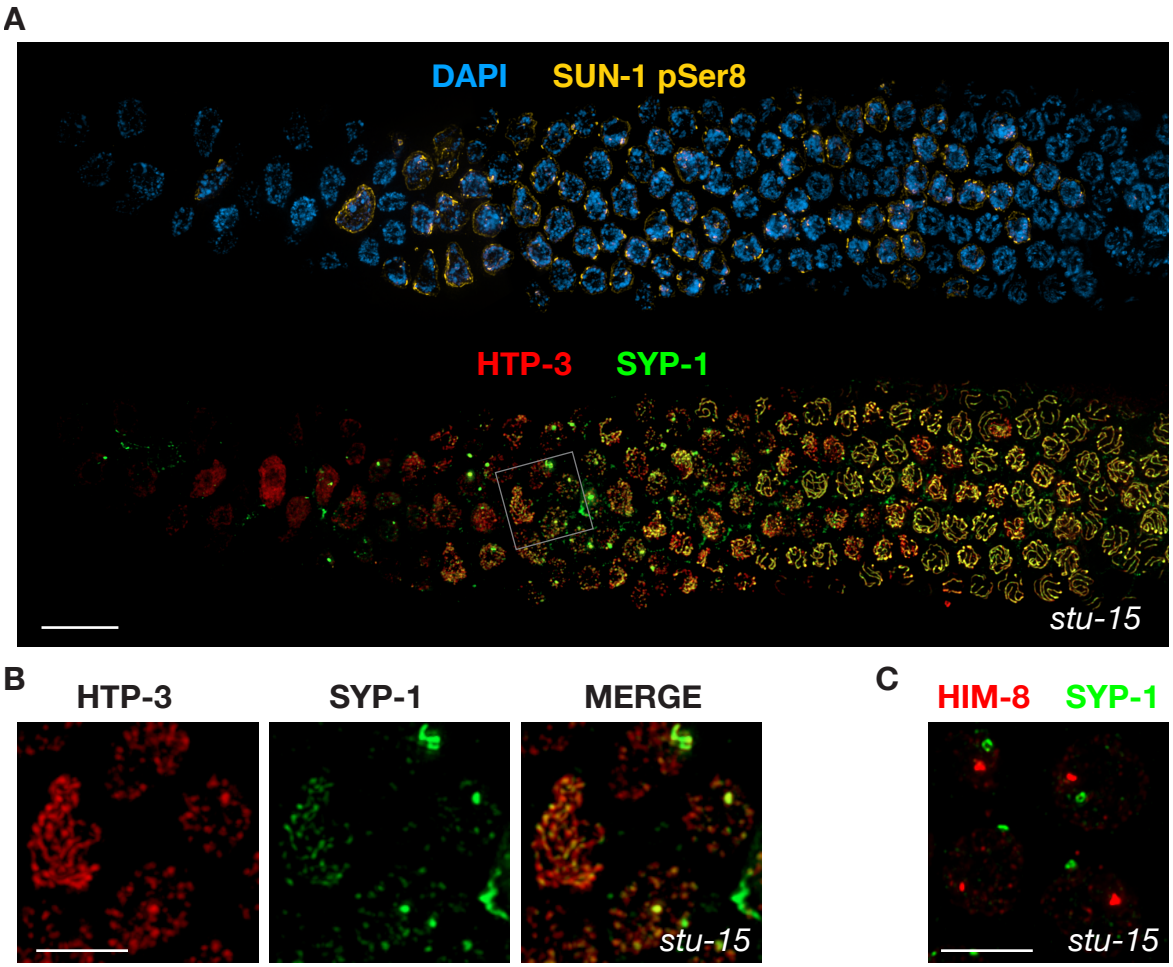

Figure 2.5 *stu-15* animals exhibit defects in chromosome axes formation (A) Composite projection images of a gonad from a *stu-15(oj28)* animal that was shifted to 25˚C at the L4 stage for 48 hours and stained with DAPI, anti-SUN-1 Ser8-Pi (yellow), anti-HTP-3 (red), and anti-SYP-1 (green). Separate images are shown for DAPI and SUN-1 staining and for HTP-3 and SYP-1 staining. Meiotic progression is from left to right. Nuclei from distal tip to late pachytene are shown. An extended transition zone as well as extensive asynapsis is present in *stu-15 (oj28)* mutants. Scale bar, 15µM (B) Higher-magnification of nuclei stained with anti-HTP-3 and anti-SYP-1 is shown. HTP-3 fails to load properly in a significant number of nuclei during early prophase, forming foci along chromosomes that associate with SYP-1. SC polycomplexes are also formed in *stu-15(oj28)* mutants. Scale bar, 5µM. (C) Field of meiotic nuclei from *stu-15(oj28)* mutants stained with anti-HIM-8 (chromosome PC ZnF protein, red) and anti-SYP-1 (central element protein, green) X chromosomes are paired but unsynapsed during early prophase of *stu-15(oj28)* mutants. Scale bar, 5µM.

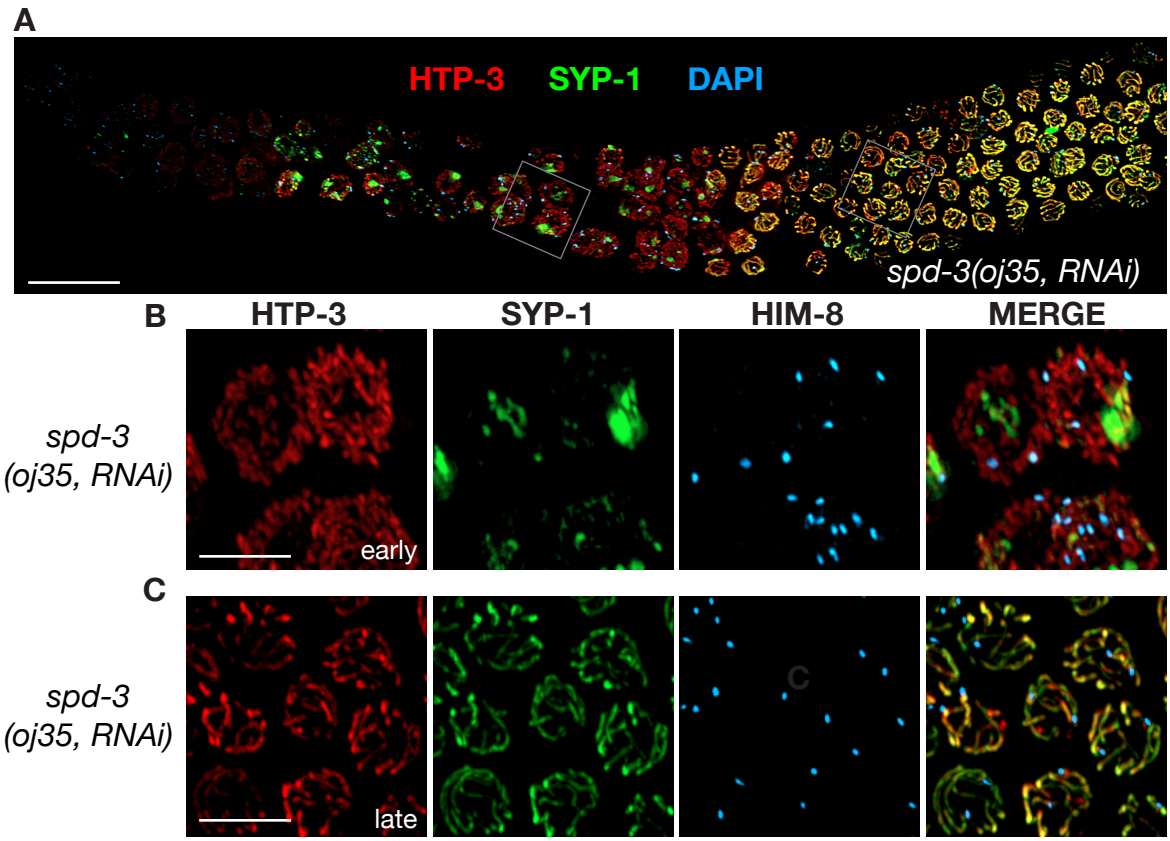

Figure 2.6 *spd-3(oj35, RNAi)* mutants exhibit nonhomologous synapsis (A) Composite projection images of a gonad from a *spd-3(oj35, RNAi)* animal stained with anti-HTP-3 (axial element protein, red), anti-SYP-1 (central element protein, green) and anti-HIM-8 (X chromosome PC ZnF protein, blue). Nuclei from the distal tip up to late pachytene. Meiotic progression is from left to right. Scale bar, 15µM. (B) Higher-magnification of early prophase nuclei is shown. Multiple HIM-8 foci are present, chromosomes fail to synapse and SC polycomplexes are present in *spd-3(oj35,RNAi)* mutants. Scale bar, 5µM. (C) Higher magnification of mid-pachytene nuclei is shown. Most nuclei achieve complete synapsis but X chromosomes remain unpaired.

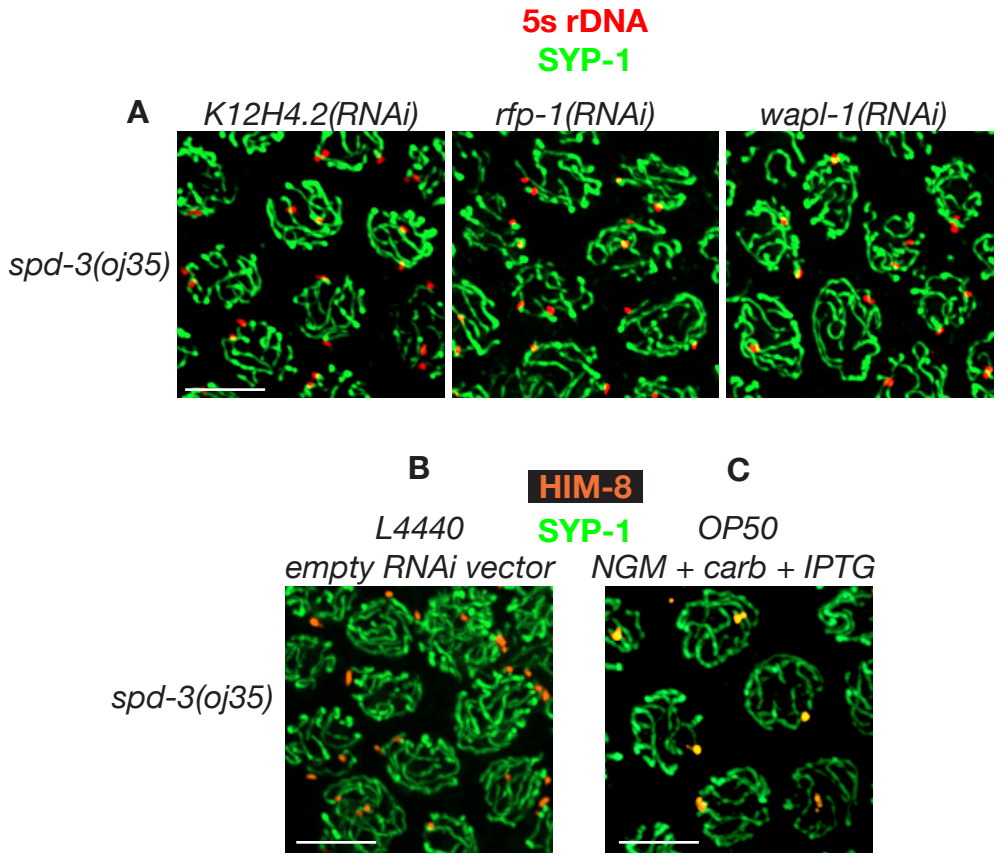

Figure 2.7 Bacterial diet influences meiosis in *spd-3(oj35)* animals (A) Field of pachytene nuclei from *spd-3(oj35)* animals fed with HT115 bacteria expressing various dsRNA, stained with anti-SYP-1 (central element, green) and marked by FISH with a probe against 5s rDNA (chromosome V, red). Unpaired chromosome V associates with SYP-1 tracks in each mutant background. Scale bar, 5µM. (B) Field of pachytene nuclei from *spd-3(oj35)* animals fed with HT115 bacteria containing the empty RNAi vector L4440 and stained with anti-SYP-1 and anti-HIM-8 (X chromosome PC ZnF protein, orange). Unpaired X chromosomes associate with SYP-1 tracks. (C) Field of pachytene nuclei from *spd-3(oj35)* animals fed OP50 bacteria on an NGM plate containing carbenicillin and IPTG and stained with anit-SYP-1 and anti-HIM-8. X chromosome pairs and synapses like wild-type.

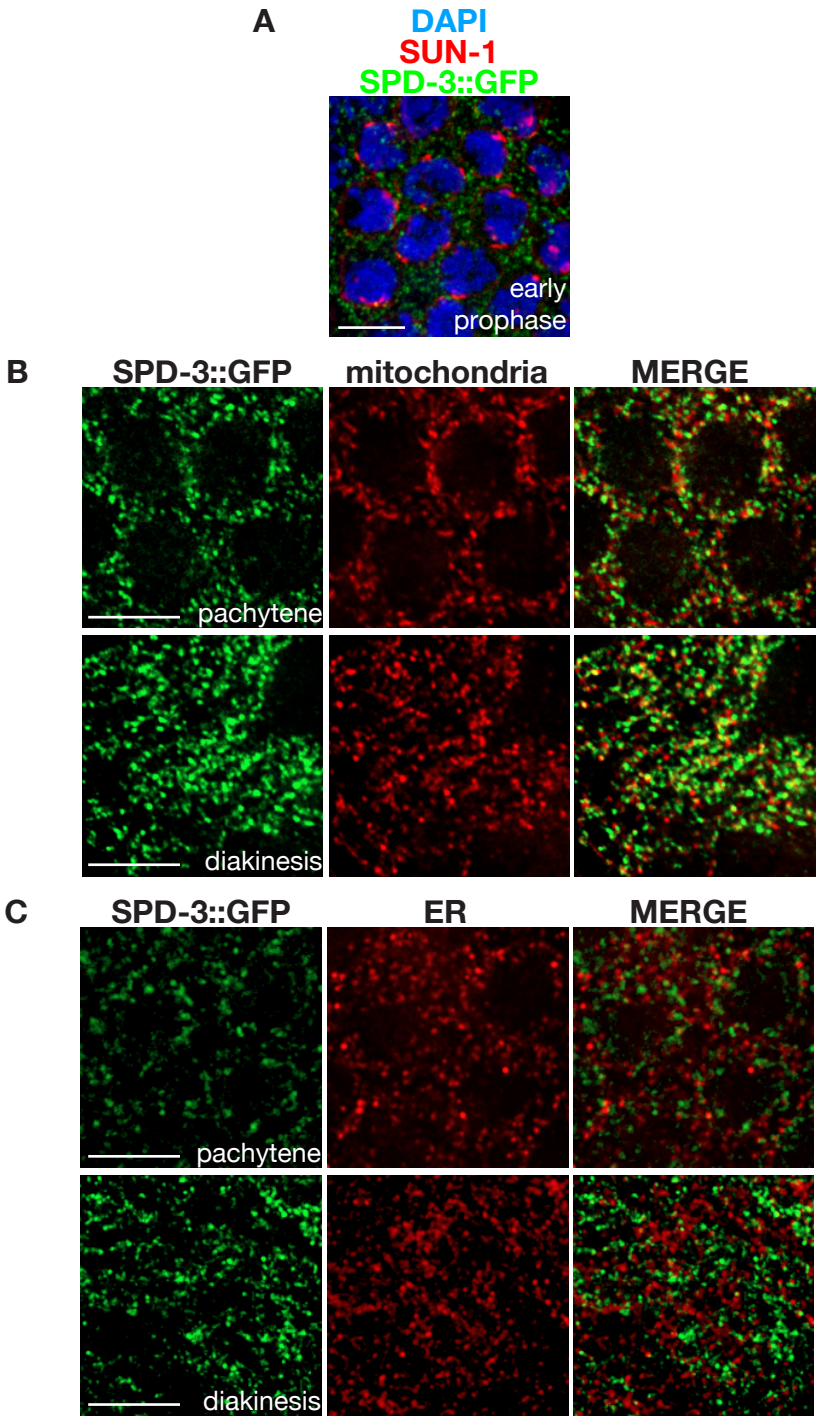

Figure 2.8 Subcellular localization of SPD-3 in the germline (A) Projection of maximum-intensity 3D images of early prophase nuclei from *oj33* animals expressing *spd-3::gfp* stained with anti-GFP (SPD-3, green), anti-SUN-1 (nuclear envelope patch component, red) and DAPI (chromosomes, blue). SPD-3 localizes outside of germline nuclei, exhibiting a punctate pattern all over the cytoplasm,

and does not colocalize with SUN-1 at the nuclear envelope. Scale bar, 5µM. (B) and (C) Field of nuclei in pachytene (top panel) and diakinesis (bottom panel) are shown from an *oj33* animal that was stained with anti-GFP and antibodies against mitochondrial proteins or the ER retention signal (see Materials and Methods, red). (B) SPD-3 does not localize to the mitochondria. (C) SPD-3 does not localize to the ER. Scale bars, 5uM.

Genomic Position and Strain Name	*Mos1* allele	Primers for L homologous region	Primers for R homologous region	Allele
X PC IE9551	*ttTi9551*	F:cagacgaactcgctagaccgatc R: cggaatgataccacttcttaa	F:aaaagggctcgtcaaaatgagagag R: ccctttcagcatcgaccacggc	*ieSi2*
X non-PC IE1565	*ttTi1565*	F:ggggacaactttgtatagaaagttg R: gggactgtttttgtacaaacttg	F: ggggacagctttcttgtacaaagtgg R: gggacaactttgtataataaagttg	*ieSi3*
III PC IE713	*ttTi713*	F: gagcttgtcacgtctgctg R:gggagaatgactaaatccacctatt	F: taagtgaaaatgtcattttctctcg R: gctgcagtatgacgtcacaac	*ieSi5*
III non-PC IE25678	*ttTi25678*	F: caaagagcaaatgggcaac R: agtttcgtaatttttaaaaggg	F: tatggttttccaagtgatatgtc R: ccaaattgttggtaaactgcc	*ieSi18*

Table 2. LacO array insertion strains generated by MosSCI. Primer pairs were used to amplify homologous sequences flanking the Mos1 insertion.

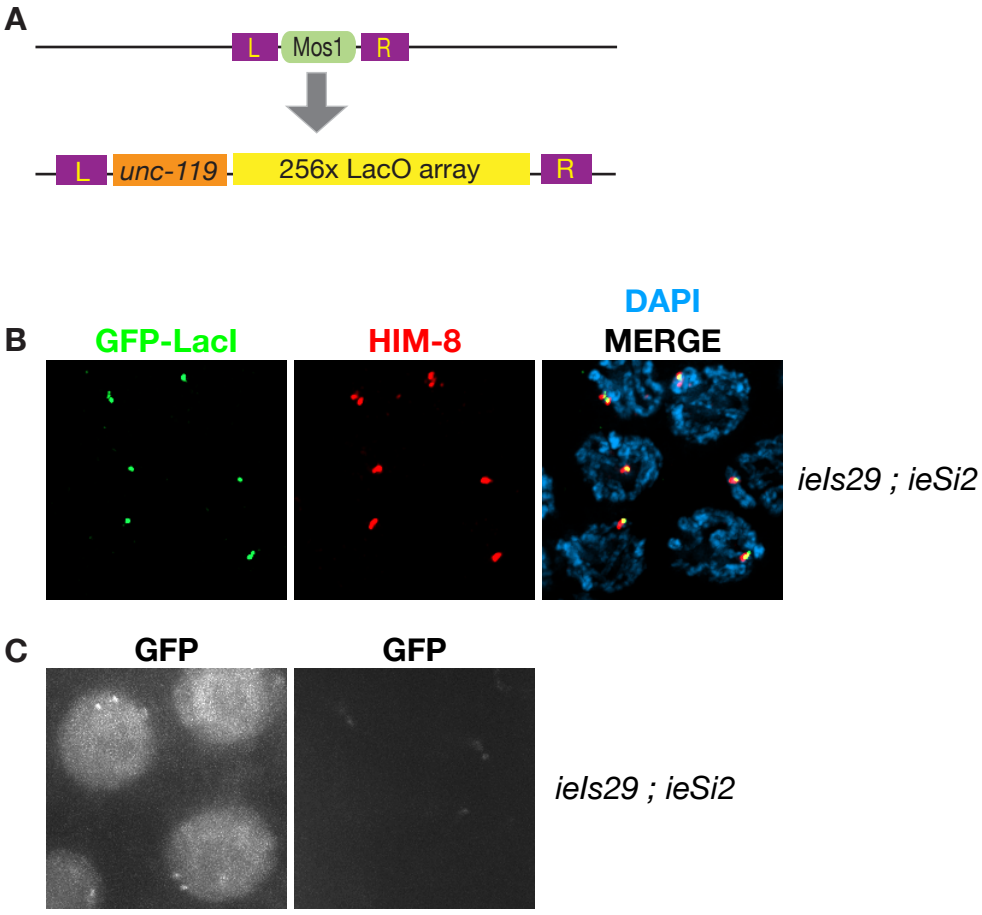

Figure 2.9 Implementing the LacI/LacO system for live imaging of meiotic chromosomes. (A) A schematic of the LacO array insertion at the *Mos1* element site generated by *MosSCI.* (B) GFP-LacI binds to the LacO array inserted at the X chromosome Pairing Center. Images are maximum-intensity projections from 3D stacks showing a field of pachytene nuclei in *ieIs29 [cb unc-119+; Pzyg-12::gfp::lacI]; isSi2 [cb unc-119+; LacOx256]* animals. (C) Partial projections through a field of pachytene nuclei in *ieSi29; ieSi2* animals. Image on the right was captured in an animal of the same genotype but several generations later. GFP foci are very dim and nuclear GFP signal is completely absent.